Journal of Molecular Liquids 424 (2025) 127021

Contents lists available at ScienceDirect

Journal of Molecular Liquids

journal homepage: www.elsevier.com/locate/molliq

Spontaneous in-situ emulsification and enhanced oil recovery using functionalised silica nanoparticles: Insights from spontaneous imbibition and micromodel flooding tests

Louey Tliba [a], Mohamed Edokali [a], Thomas Moore [b], Omar Choudhry [d], Paul W.J. Glover [c], Robert Menzel [b], Ali Hassanpour [a,*]

[a] School of Chemical and Process Engineering, Faculty of Engineering and Physical Science, University of Leeds, Leeds LS2 9JT, UK
[b] School of Chemistry, Faculty of Engineering and Physical Science, University of Leeds, Leeds LS2 9JT, UK
[c] School of Earth and Environment, University of Leeds, Leeds LS2 9JT, UK
[d] School of Computing, University of Leeds, Leeds LS2 9JT, UK

ARTICLE INFO

Keywords:
Enhanced oil recovery
Grafting
Spontaneous imbibition
Microfluidic performance
Emulsion stability
Wettability alteration

ABSTRACT

This study investigates the potential of functionalised silica nanoparticles (SiO_2 NPs) for enhanced oil recovery (EOR), employing environmentally friendly and cost-effective materials. SiO_2 NPs were optimally modified with ammonium lauryl sulfate (ALS) and sodium (C14-16) olefin sulfonate (SOS) surfactants under optimal conditions without binding agents, representing their first application in EOR. Characterisation techniques, including Fourier-transform infrared spectroscopy (FTIR) and thermogravimetric analysis (TGA), confirmed the effective functionalisation of SiO_2 NPs. Transmission electron microscopy (TEM) images revealed that the morphology, structure, and shape of the NPs remained unchanged post-functionalisation, with an average diameter of 20 nm. The performance of ALS-NPs and SOS-NPs was assessed through spontaneous imbibition and microfluidic tests. ALS-NPs and SOS-NPs achieved oil recovery rates of approximately 66 % and 70 %, respectively, in spontaneous imbibition tests. Microfluidic model tests corroborated these findings, with oil recovery rates of approximately 74 % for ALS-NPs and 80 % for SOS-NPs. Both functionalised nanofluids demonstrated superior oil recovery compared to surfactants alone and non-functionalised SiO_2 NPs. The application of these nanofluids facilitated the spontaneous formation of smaller, more stable emulsion droplets, enhancing displacement efficiency and reducing pore blockages. Moreover, the nanofluids improved oil recovery by reducing interfacial tension (IFT), altering rock wettability, and forming stable oil-in-water emulsions. The grafting approach of ALS- and SOS-based nanofluids demonstrates greater efficiency by requiring lower surfactant concentrations, thereby making the process cost-effective.

1. Introduction

The rising global demand for energy has intensified the need to maximise oil recovery from existing reservoirs [1–4]. Among the advanced recovery methods, chemical enhanced oil recovery (cEOR) stands out as a promising technique that leverages surfactants, polymers, and alkalis to improve oil displacement and sweep efficiency [5,6]. By reducing oil–water interfacial tension (IFT) and increasing the viscosity of the displacing fluid, cEOR enhances both microscopic and macroscopic oil recovery [7,8]. Recent research has extensively investigated ionic, non-ionic, and amphoteric surfactants for their role in enhancing residual oil recovery [9,10]. For instance, cationic surfactants have shown significant efficacy in carbonate reservoirs, while anionic surfactants are more suitable for sandstone reservoirs [9,10]. These surfactants function by altering the wettability of reservoir rocks, micro-emulsifying trapped oil, and improving interfacial rheology.

Abbreviations: ALS, Ammonium lauryl sulfate; BET, Brunauer–Emmett–Teller; BS, Brine solution; cEOR, Chemical enhanced oil recovery; DLS, Dynamic Light Scattering; DW, Deionised water; EOR, Enhanced Oil Recovery; FTIR, Fourier Transform Infrared spectroscopy; IFT, Interfacial tension; LSW, Low salinity water; NPs, Nanoparticles; SEM, Scanning Electron Microscope; SI, Supporting Information; SiO_2, Silica nanoparticle; SOS, sodium (C14-16) olefin sulfonate; TEM, Transmission Electron Microscopy; TGA, Thermo-gravimetric analysis; ZP, Zeta Potential.

* Corresponding author.
E-mail address: a.hassanpour@leeds.ac.uk (A. Hassanpour).

https://doi.org/10.1016/j.molliq.2025.127021
Received 18 October 2024; Received in revised form 14 January 2025; Accepted 24 January 2025
Available online 24 January 2025

Surfactants typically facilitate emulsification at the oil–water interface by reducing IFT through diffusion and stranding effects. This mechanism often leads to the formation of water-in-oil emulsions, particularly in asphaltene-rich oils [11–13]. The spontaneous formation of micro-emulsions plays a critical role in expanding connate water, thereby mobilising trapped oil [13,14]. However, the application of surfactants faces challenges such as high costs, stability issues under reservoir conditions, and the risk of exceeding the critical micelle concentration (CMC), which can lead to micelle formation and decreased efficiency [5,9,15,16].

For example, Qazi et al. demonstrated that Cetyltrimethylammonium bromide (CTAB), a cationic surfactant, reduces IFT and improves the mobility ratio in cEOR applications [17]. However, at concentrations beyond the CMC, micelle formation shifted the mechanism from diffusion-controlled to adsorption barrier-controlled processes, diminishing surfactant efficacy [15,16]. To address these challenges, researchers have explored the use of nanoparticles (NPs) as nanocarriers for surfactants through functionalisation [15,18].

Surfactant-functionalised NPs can enhance IFT reduction and improve the rheological properties of fluids, even under harsh reservoir conditions such as high temperature and salinity [19–22]. The NPs not only concentrate surfactants at the interface [19,20], but also act as protective agents, minimising surfactants adsorption on rock surfaces and prevent degradation [19,23,24]. Moreover, the incorporation of NPs with surfactants has been shown to improve emulsion stability in EOR applications [25,26]. The effectiveness of NPs at the oil–water interface depends on their size, type, and concentration [19,27]. Smaller NPs exhibit superior emulsion stability due to their ability to form dense interfacial films that effectively prevent droplet coalescence [19,26,27]. Several studies have highlighted the synergistic effects of surfactants and Silica (SiO_2) NPs. For instance, Wang et al. reported that combining SiO_2 NPs with alkaline-surfactant-polymer (ASP) solutions and SiO_2 NPs reduced IFT and improved oil displacement efficiency, enhancing oil recovery by approximately 7 % of the original oil in place (OOIP) [28]. Similarly, Lhekoronye et al. observed that the combination of biosurfactants and NPs in the Niger Delta oil fields significantly increased oil recovery rates by altering the wettability and reducing IFT [29]. Further, Razaei et al. demonstrated that alpha-olefin sulfonate (AOS) surfactant combined with hydrophilic SiO_2 NPs significantly improved oil recovery in carbonate reservoirs [30]. However, despite these advancements, challenges remain. Physical mixing of NPs with surfactants without functionalisation, can lead to aggregation under reservoir conditions, potentially blocking pores and compromising reservoir permeability. Therefore, optimising NPs-surfactant interactions is essential to mitigate aggregation and ensure stable, efficient EOR processes. For instance, Mingwei et al. functionalised modified SiO_2 NPs with lauramidopropyl hydroxy sulfobetaine surfactant, producing a stable nanofluid that improved oil recovery during spontaneous imbibition tests [31]. Similarly, Ganesh et al. developed a nanofluid using positively charged Ludox CL SiO_2 NPs and Aerosol-OT (AOT) surfactant, which effectively reduced IFT and altered the sandstone core wettability, resulting in enhanced oil recovery [32].

These recent studies have demonstrated the effectiveness of combining SiO_2 NPs with surfactants to enhance oil recovery. However, one of the limitations is that SiO_2 NPs require primary grafting before being functionalized with surfactants. Furthermore, limited research has explored the phase behaviour of nanofluids through spontaneous emulsion formation, a mechanism recently recognised as a crucial for oil recovery [33]. Understanding the stability and dispersion of emulsions within porous media is, therefore, essential for the effective implementation of EOR [34]. Consequently, there is a strong demand for optimising cost-effective and environmentally friendly EOR technologies.

This study aims to address these challenges by introducing a systematic approach to identify the most suitable surfactants and study their behaviour and mechanism in enhancing oil recovery using SiO_2 NPs. Herein, commercially available SiO_2 NPs functionalised were modified with two specific anionic surfactants: ammonium lauryl sulfate (ALS) and sodium (C14-16) olefin sulfonate (SOS). These surfactants were selected from a comprehensive range of cationic, anionic, and non-ionic options based on phase behaviour studies. To the best of our knowledge, this is the first application of ALS and SOS as EOR agents and modifiers for SiO_2 NPs. The modified SiO_2 NPs were employed as surfactant nanocarriers via a simple one-step modification process, significantly reducing the required concentrations of surfactants and NPs compared to complex multi-step procedures commonly reported in the literature. A variety of characterisation methods were used to examine the morphology, surface properties, functionality, and the stability of the NPs. These methods included Transmission electron microscopy (TEM), Thermogravimetric analysis (TGA), Fourier-transform infrared spectroscopy (FTIR), Brunauer–Emmett–Teller (BET), Zetasizer, and Dynamic Light Scattering (DLS). The oil in water emulsions were prepared in the absence and presence of alkali to identify optimal alkali concentration, with emulsion stability evaluated through droplet size distribution, and IFT measurement. Moreover, oil displacement tests employing spontaneous imbibition tests were conducted on saturated Berea sandstone cores. Furthermore, the movement and interaction of these NPs within a physically modelled sandstone microchip were analysed using custom-developed software that integrates advanced statistical modelling and automated image processing workflow (an OpenCV framework coupled with dynamic thresholding and Gaussian blurring). The purpose of these tests was to evaluate the synergistic effectiveness of the novel nanofluid in improving oil recovery and to assess the performance of the generated oil/water emulsions, resembling EOR mechanisms at the pore scale.

2. Materials and methods

2.1. Materials

In this study, a variety of surfactants were utilised to identify the optimal candidate for modifying the surface of SiO_2 NPs to generate nanofluids. The tested surfactants included dodecyl benzene sulfonic acid (DBSA), sodium dodecyl benzene sulfonate (SDBS), sodium lauryl sulfate (SLS), ammonium lauryl sulfate (ALS), cetyltrimethylammonium bromide (CTAB), tween 80-surfactant, polyvinylpyrrolidone (PVP, M.W. 40,000). These were purchased from Sigma-Aldrich and used without any modification. Additionally, sodium (C14-16) olefin sulfonate (SOS), and isoproylamine dodecylbenzene sulfonate (IDS) were supplied by Stepan company. Various salts with 99 % purity were used in this study without purification, all of which were procured from VWR. These salts included sodium carbonate, magnesium chloride, calcium chloride, sodium chloride, and potassium chloride. Deionised water (DW) was employed as the dispersing medium for the preparation of NPs throughout the study. To accurately simulate oil reservoir conditions, Algerian dead crude oil was utilised, characterised by an API gravity of 24.6, a viscosity of 71 cP at room temperature and 13 cP at 60 °C, and an asphaltene content of 0.25 %. This oil was used for performance testing throughout the study. Furthermore, Berea sandstone cores were employed to model the reservoir environment, with porosity ranging from 20 % to 22 %.

2.2. Brine Solution

Our previous research has demonstrated that optimal salinity levels in water significantly influence the stability, dispersion, and transport of NPs within reservoirs, thereby enhancing oil recovery efficiency [35]. To identify the most suitable dispersant for the nanofluid, various NaCl concentrations ranging from 0 to 2 wt% were examined through zeta potential measurements using 0.5 g of sand. The concentration that yielded the highest zeta potential (with NaCl at 500 ppm) was selected as the dispersant for all solutions prepared in this study and was

designated as LSW (see Fig. S1) [35].

2.3. Preparation of emulsions with varying oil-to-water ratios

Emulsions were prepared with varying oil-to-water ratios of 1:1, 1:2, 1:4, and 1:9, in order to study the effect of oil-to-water ratio on emulsion stability (see Fig. S2). All the o/w ratios exhibited a clear phase separation immediately after mixing. However, the emulsion with a 1:9 oil-to-water ratio demonstrated a more desirable emulsion compared to those with higher oil contents. Consequently, all in-situ oil/water emulsions in this study were prepared using the optimal 1:9 ratio. This was achieved by combining 3 ml of crude oil to 27 ml of LSW.

2.4. Preparation of emulsions with sodium carbonate

Alkaline substances have the ability to interact with acidic elements found in crude oil, including asphaltene, naphthenic acids, and fatty acids, leading to alterations with interfacial properties and aiding in the reduction of IFT [36]. Various emulsions were prepared using an optimal 1:9 oil-to-water ratio with sodium carbonate concentrations ranging from 0 to 0.5 wt% to study the effect of alkali on the formation of stable, spontaneous emulsions. Fig. S3 illustrates the images captured at different time intervals to determine the most effective emulsion across the different sodium carbonate concentrations. At a concentration of 0.1 wt% sodium carbonate, a noticeable change in oil/water emulsion was observed compared to lower concentrations. However, increasing the sodium carbonate concentration beyond 0.1 wt% did not significantly enhance emulsion stability. Even at 0.5 wt%, the emulsion was comparable to that observed at 0.1 wt%. This result suggests that a sodium carbonate concentration exceeding 0.1 wt% does not further enhance the formation of stable oil/water emulsions. Consequently, this concentration was selected for subsequent emulsion preparation processes.

2.5. Nanoparticle modification and characterisation

In this study, commercially available SiO_2 nanoscale powder (10–20 nm particle size, with 99.5 % purity) was used. Initially, 1 g of SiO_2 NPs was modified with ALS surfactant, employing varying surfactant concentrations. The procedure and characterization for determining the optimal surfactant/SiO_2 ratio are summarised in Section SI3 of the Supporting information (SI). A 1.5/1 g ratio was subsequently selected for grafting SiO_2 NPs with ALS and/or SOS surfactant. Experimentally, 1 g of SiO_2 NPs was dispersed in 100 ml of DW and stirred at 300 rpm for 30 min at 60 °C (Solution 1). Separately, 1.5 g of ALS was added to 50 ml of DW and stirred gently at 100 rpm for 1 h at 60 °C (Solution 2). Solution 1 was then gradually added dropwise to Solution 2 over 15 min to promote in-depth interaction of ALS with the SiO_2 NPs surface. The resultant mixture was stirred continuously for 24 h at 120 rpm and 60 °C. Following this, the mixture was centrifuged at 5000 rpm for 15 min, and the supernatant was decanted. The precipitate was recovered and washed three times to remove any unbound ALS molecules, then frozen for 10 min in a liquid nitrogen bath (−196 °C) and placed in a freeze-dryer for 48 h to sublimate the frozen water. The resulting sample was labelled as ALS-NPs. This procedure was repeated with surfacatnt with SiO_2 NPs, with the resulting sample being identified as SOS-NPs. Subsequently, several characterisation techniques were employed to confirm the successful grafting of these agents onto the surface of the SiO_2 NPs and to assess their functionality, surface area, and morphology before and after grafting.

2.5.1. Thermo-gravimetric analysis (TGA)

The amount of ALS and SOS grafted onto the surface of the NPs was determined using a Mettler Toledo TGA/DSC1 instrument. Solid-state samples were analysed without prior purification. Approximately 10 mg of each sample was placed in a 70 μL alumina crucible and positioned in the TGA/DSC1 sample holder. The TGA analysis was conducted over a temperature range of 30 °C–900 °C, with a heating rate of 10 °C/min under a steady airflow of 50 ml/min.

2.5.2. Fourier transform infrared spectroscopy (FTIR)

A ThermoFisher Scientific Nicolet iS10 FTIR spectrometer was employed to identify the primary functional groups and molecular bonds in SiO_2 NPs, both before and after functionalisation with ALS and SOS agents. Sample preparation involved mixing 6 mg of each sample with 500 mg of KBr, followed by placing the mixture in a DRIFTS holder. The analysis was performed in transmission mode across a spectral range of 400–4000 cm^{-1}, with a resolution of 2 cm^{-1}. The final spectrum was averaged over 128 scans to ensure accuracy and reproducibility.

2.5.3. Brunauer–Emmett–Teller (BET)

The Brunauer–Emmett–Teller (BET) gas adsorption–desorption method (Micromeritics Tristar 3000) was employed to evaluate the impact of ALS and SOS loading on the surface properties of virgin SiO_2 NPs. This technique is critical for assessing porous materials, including the surface area and porosity of micro- and mesoporous structures. The samples were analysed in their solid form. Initially, they were degassed using a Micromeritics Flow Prep 060 sample degas system under nitrogen (N_2) gas flow, heated to 423 K overnight to remove moisture and impurities from the surface and pores. Following degassing, the samples were weighed to ensure accurate calculations by the software. Subsequently, the samples were subjected to nitrogen adsorption–desorption at 77 K to produce adsorption–desorption isotherms.

2.5.4. Transmission electron microscopy (TEM)

TEM analysis was used to assess the morphology, size, and structural changes of SiO_2 NPs before and after the functionalisation with ALS or SOS agents. TEM measurements were performed using the FEI Titan Themis Cubed, operated at 300 kV and equipped with a monochromator. Samples were prepared by suspending the NPs in 5 ml of DW *via* ultrasonication. A droplet of the suspension was then placed on a carbon-coated copper grid and allowed to dry completely. Bright-field TEM images were captured using a Gatan OneView 16Megapixel CMOS digital camera with a 2 nA screen current. Elemental analysis was conducted using a super-X EDX system equipped with four windowless detectors, and spectra were acquired in TEM mode using Velox software.

2.6. Characterisation of nanofluids

2.6.1. Zetasizer and dynamic Light Scattering (DLS)

Zeta potential analyses were performed using the Malvern Zetasizer Nano ZS/ZSP instrument (MRK654-01) to evaluate the stability and surface charge of the prepared nanofluids at room temperature. Z-potential measurements were conducted using the Zetasizer software, employing the Smoluchowski approximation for aqueous systems, with a 60-second equilibration time at ambient temperature in automatic processing mode. The concentration of the nanofluid selected for these measurements was 100 ppm, based on screening studies from the IFT measurements and the prepared nanoemulsions, as detailed in section 2.7. To examine the effect of the selected alkali concentration on nanofluid stability, ZP/DLS measurements were conducted before and after the addition of 0.1 wt% alkali, with N1 and N2 representing the selected nanofluids without and with alkali, respectively. A small volume of nanofluid was introduced into 1 ml disposable cells using a syringe. The instrument was configured to take three measurements per sample, and an arithmetic average was calculated. To ensure reproducibility, the measurements were repeated three times, and the average ZP values were recorded. Additionally, the size distributions of the selected nanofluids were determined using dynamic light scattering (DLS) on the same instrument.

2.6.2. Interfacial tension (IFT) measurements

A series of Interfacial tension (IFT) experiments between oil and diversely prepared nanofluids was carried out: (i) to compare the efficacy of modified SiO_2 NPs with ALS and SOS in reducing IFT for stabilising oil/water emulsions relative to virgin SiO_2 NPs, and (ii) to determine the optimal concentration of nanofluids for further investigation, including EOR-applications. Nanofluids concentrations ranging from 10 to 500 ppm were prepared for these measurements.

The IFT measurements were performed at room temperature using the pendant drop method with a Biolin Scientific Attension Theta Flex Optical Tensiometer. A droplet of crude oil was generated at the tip of a hooked needle within a chamber containing the nanofluid, and the IFT between the oil droplet and the various nanofluid formulations was recorded over a time interval of 2000 s. Due to instrument measurement limitations, it was not possible to measure IFT following alkali addition or at concentration above 500 ppm for the ALS-NPs and SOS-NPs.

2.7. Characterisation of nanoemulsions

As previously mentioned, emulsions were prepared by gently mixing 3 ml of crude oil with 27 ml of differently prepared nanofluids to formulate in situ oil/water emulsions. These nanofluids were prepared with concentrations ranging from 0.001 wt% to 0.4 wt%. The main objectives of this work were: (i) to compare the effectiveness of modified SiO_2 NPs with ALS and SOS surfactants in formulating stable in situ oil/water emulsions relative to surfactants alone; and (ii) to determine the optimal concentration of nanofluid that best stabilises the nanoemulsions. The prepared emulsions were characterised using different methods. Initial visual inspections were conducted, followed by the calculation of the creaming degree (CD %) after allowing the emulsions to settle for approximately two weeks [37–39]. Three measurements were averaged for each sample. This measurement evaluates the volume fraction of oil that separates from the total initial volume of the emulsion, providing an overall indication of the nanofluid's effectiveness in stabilizing oil/water emulsions. Generally, a creaming degree close to 0 % indicates a stable oil/water emulsion, signifying minimal or no separation of the oil phase from the water phase [37–39]. However, a creaming degree close to 100 % indicates emulsion instability, with a large quantity of oil separating and rising to the top of the vial [37–39]. Following this evaluation, an optimum nanofluid concentration for both ALS-NPs and SOS-NPs was selected for further characterisation. This included the droplet size measurements of the emulsion and microscope examinations, compared to emulsions stability by surfactants alone at the same concentration. Particle size distributions of emulsions were determined at 25 °C using a Malvern MasterSizer 3000 (Malvern Instruments Ltd, Malvern, Worcestershire, UK) in conjunction with a Malvern Hydro MV dispersion unit. The selected samples were diluted in DW to achieve an obscuration of between 4 % and 6 %. Stirring speed was set as 1000 rpm, and measurements were repeated three times to obtain an average droplet size distribution. Subsequently, the selected emulsions were visualised using an Olympus BX51 optical microscope equipped with a digital camera at 50× magnification. Both techniques were employed to compare of emulsions sizes before and after the inclusion of the prepared nanofluid at their optimal concentration.

2.8. Enhanced oil recovery (EOR) measurements

2.8.1. Contact angle measurements

Contact angle measurements were conducted to quantitatively evaluate the wettability of the core samples using a Biolinc Scientific Attension Theta Flex optical tensiometer. Sandstone cores were polished and shaped to fit within a cubic chamber, then aged in crude oil for approximately one week at 70 °C under atmospheric pressure. This aging process was designed to alter the wettability of the cores, simulating oil-wet reservoir conditions. The substrates were subsequently dried in an oven at 60 °C for six hours [40]. Wettability evaluations began with oil droplet tests conducted before and after the aging process. The oil-aged cores were then immersed in various fluids at 60 °C for two days [40]. After immersion, each substrate was dried in an oven at 55 °C for two hours. Contact angle measurements were performed to assess the impact of the nanofluids on wettability alteration.

2.8.2. Spontaneous imbibition test

Prior to conducting the spontaneous imbibition test, a Berea sandstone core plug with a diameter of 3.8 cm and a length of 30 cm was sectioned into smaller plugs, each approximately 4.1 cm in length. The porosity of these cores was evaluated at 22 °C using the helium gas expansion method. Table 1 summarises the petrophysical characteristics of the core samples used in this study. Spontaneous imbibition tests, which are static methods, were employed to evaluate the efficacy of the prepared nanofluids for EOR. These tests aimed to identify the mechanisms responsible for EOR. The experiments were conducted in high-temperature Amott cells with a volume capacity of approximately 400 ml [35]. These cells were equipped with graduated glass tubes to facilitate the direct measurement of oil recovery from the core samples. The recovery factor was calculated based on the maximum oil volume extracted over a given period. It is worth noting that all spontaneous imbibition tests were performed without any initial water saturation [41]. The experimental procedure comprised several stages, as detailed Section (SI4) and in our previous study [35]. All imbibition tests were carried out at 60 °C and continued until no further oil could be recovered [35]. The volume of oil expelled from the cores was measured to determine the oil recovery as a percentage of the original oil in place (% OOIP), using the equation provided below [31,35]:

$$OR = \frac{V_o \rho_o}{M} \times 100\% \quad (1)$$

where: OR refers to the percentage of oil recovery, V_o indicates the volume of oil released from the cores, ρ_o is the crude oil density, and M represents the mass difference of the cores before and after oil saturation.

2.8.3. Micromodel flooding test

Flooding experiments were conducted using a microfluidic device to evaluate the efficacy of EOR at the pore scale, both in the absence and presence of NPs. This method enables direct observation of fluid flow and is more efficient than traditional core flooding tests, as it requires smaller fluids volumes [42,43]. The microfluidic device enables direct visualisation of oil recovery, facilitating the identification of mechanisms responsible for oil displacement following nanofluid injection [42,44]. The microchips, along with the chip holder and micromodel connections, were sourced from Micronit, Enschede, the Netherlands. Fig. 1 and S6 show schematic diagram of the micromodel setup used for flooding experiments including the oil-wet microchips with physical rock networks utilised in this study. These microchips are designed with random rock-shaped structures to closely simulate natural porous media (see Fig. 1b).

The microfluidic setup includes CETONI Nemesys Low pressure with a dual drive system and Harvard PHD 4400 syringe pumps (5 ml capacity), connected to the microchip *via* PTFE tubing with 1.6 mm outside diameter and 0.8 mm inside diameter. Ferrules were used at the tubing ends to ensure secure connections and prevent leakage. Effluents were collected through a glass tube attached to the microchip. A Zeiss Stemi 508 a microscope, controlled by Zen Light software, was programmed to take scheduled images over a period of 10 h, starting from the beginning of the EOR process. The chip was mounted on a holder, and the system was evacuated using a vacuum pump with the inlet valve closed to remove the air. A 4D valve was employed to prevent air bubble formation during fluid injection. Experiments were conducted at room temperature and close to atmospheric pressure. Initially, LSW was injected followed by crude oil, until a continuous oil stream was

Table 1
The petrophysical characteristics of the cores.

Core samples	Length (cm)	Diameter (cm)	Dry weight (g)	Pore volume (cm^3)	Porosity (%)	Permeability (mD)
S1	4.15	3.826	97.21	10.578	22.175	477.67
S2	4.116	3.827	96.389	10.436	22.047	470.21
S3	4.157	3.831	97.237	10.855	22.648	481.61
S4	4.143	3.823	97.239	10.407	21.883	450.25
S5	4.138	3.825	96.699	10.297	21.661	441.57

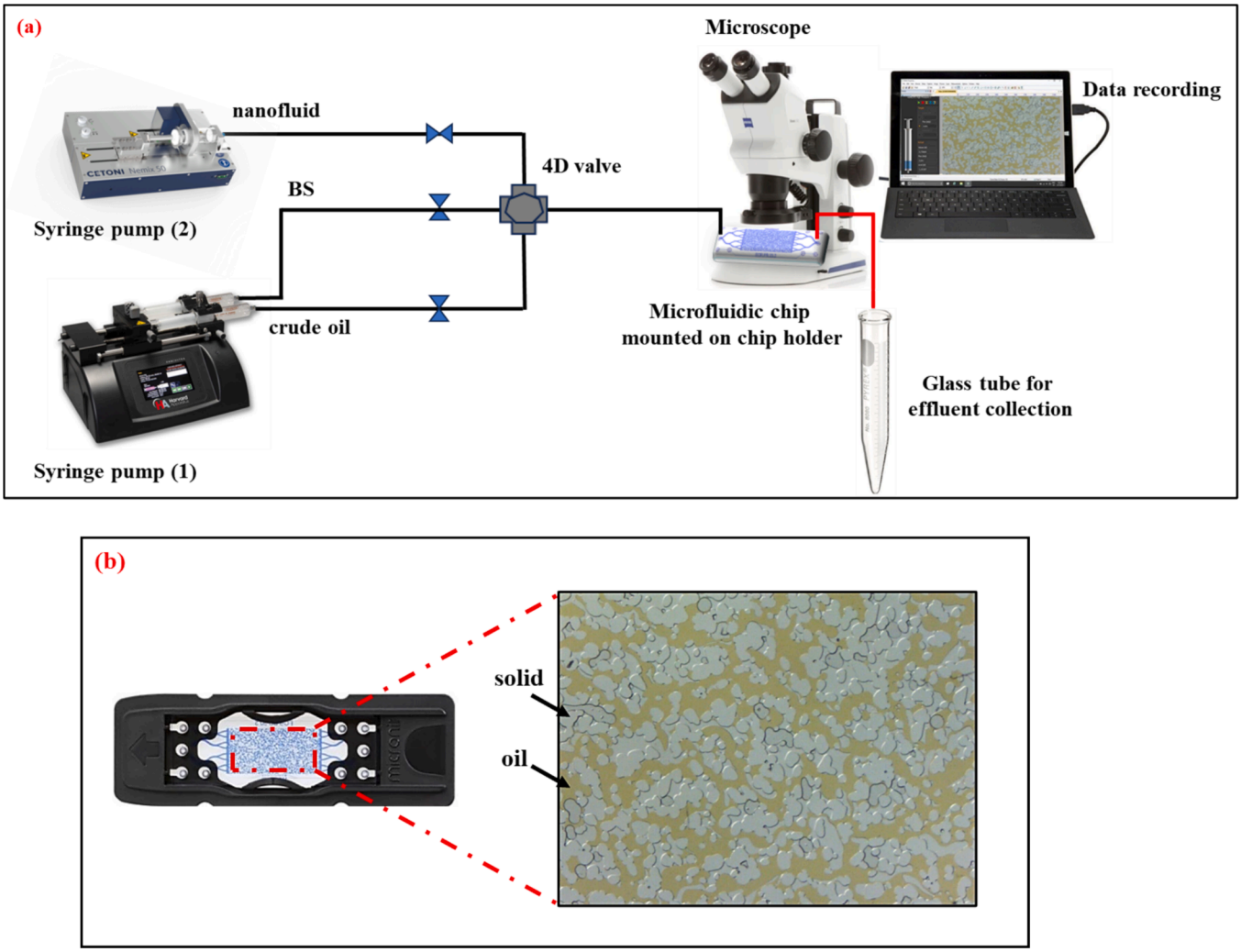

Fig. 1. (a) Schematic of the micromodel setup, (b) Image of oil-wet microchip with physical rock networks before and after crude oil saturation.

observed in the effluent collector, establishing initial water and oil saturation in the system. The experiments were conducted with a steady rate of 0.15 μl/min, equivalent to approximately 1.8 m/day in the oilfield conditions [42–44]. The LSW flooding was performed as secondary oil recovery until no further oil was extracted. Images were subsequently captured to evaluate and compare oil recovery and displacement efficiency at the start of EOR displacement tests using the different prepared surfactants and nanofluids, continuing until no additional oil production was observed.

The analysis of microscopic images in oil microchip studies has traditionally relied on tools such as ImageJ and MATLAB for image adjustment and segmentation [43]. However, this study employs advanced image processing techniques, demonstrating a robust combination of Python-based technologies and morphological operations to achieve more precise segmentation and quantification. These techniques incorporate advanced statistical modelling and automated image processing workflows, significantly improving the efficacy and scalability of oil distribution analysis over time. Specifically, the use of dynamic thresholding and Gaussian blurring within the OpenCV framework has addressed one of the major challenges reported in previous methods: the reduction of false positives and the enhancement of accuracy in distinguishing oil from other phases. Two key equations were utilised to calculate oil recovery following the flooding with various prepared fluids, as detailed below:

$$Detected\ Oil\ Ratio(DOR) = \frac{pixcelsclassifiedasoil}{totalpixcelsinimage}, and \tag{2}$$

$$OR = (1 - DOR) \times 100\%, \tag{3}$$

where DOR represents the detected oil ratio, and OR denotes the percentage of oil recovery from the cores after the imbibition test. The

calculated oil recovery percentage was then plotted over time.

3. Results and discussion

3.1. Screening of surfactants for oil with low asphaltene content

Different studies have investigated the use of different surfactants to improve the oil recovery from reservoirs [9]. In this study, Sodium lauryl sulfate (SLS) was initially chosen as an emulsifier, based on findings by Sagala et al. [16] which demonstrated its effectiveness with heavy crude oil. However, SLS was tested within this study with a type of crude oil containing approximately ten times less asphaltene than that used in their study. As illustrated in Fig. S7, SLS failed to produce stable emulsions at any concentration over a 48-h period. Consequently, a range of surfactants, including cationic, anionic, and non-ionic types was investigated to identify those most effective in forming stable oil/water emulsions with the used crude oil. Visual inspection methods were employed across concentrations ranging from 0.001 wt% to 0.3 wt%, with the selected oil: water ratio and alkali content, as illustrated in Fig. S8(a–f). The CTAB, a cationic surfactant, formed oil/water emulsions only at concentrations above its CMC, specifically around 0.2 wt% and 0.3 wt%, which induced micelle formation, making it impractical for large-scale reservoir application [9]. Non-ionic surfactants such as PVP, Tween 80, and Span 80, though recommended for EOR [9,10,45,46], failed to produce stable oil/water emulsions at any concentration.

Various anionic surfactants, including DBSA, and SDBS were also tested for their potential as effective EOR agents [9,10,45], but none resulted in stable emulsions. By contrast, the surfactants SOS and ALS demonstrated better performance in forming stable oil/water emulsions compared to other tested surfactants (see Fig. 2). Additionally, ALS and SOS, commonly used in shampoos and soap, are considered relatively eco-friendly [47–50]. Both surfactants are more cost effective than those evaluated in this study and the literature, leading their selection for further investigation.

The CMCs of ALS and SOS were determined through IFT measurements, as detailed in Section SI5. The CMC of ALS was approximately 1000 ppm, while that of SOS was around 800 ppm, consistent with values reported in the literature [51,52].

3.2. Characterisation studies for nanoparticles

3.2.1. Surfactant mass loading and functionality assessment

Some TGA analysis was performed on SiO_2 NPs both prior to and following the grafting process to quantify the content of ALS and SOS after modification. The TGA thermograms, displayed in Fig. 3a, illustrate the changes in the weight loss before and after the functionalisation of the SiO_2 NPs. The thermograms for all samples revealed two distinct weight loss regions. The first region, ranging from 25 °C to 200 °C, is associated with moisture content loss or surface dihydroxylation. The next region is from 200 °C to 800 °C, corresponding to the thermal degradation of organic compounds present on or loaded to the SiO_2 NPs surface. The virgin SiO_2 NPs lost only about 1 % under the first temperature domain, attributed to moisture loss, as shown in the Fig. 3a. However, ALS-NPs and SOS-NPs, demonstrated major mass losses of approximately 37 % and 40 %, respectively, confirming that 36 % and 39 % of the ALS and SOS surfactants used during preparation were successfully loaded onto the SiO_2 NPs.

Some FTIR measurements were conducted on the prepared NPs before and after grafting in order to further examine surface functionalities. These measurements confirmed the successful functionalisation of the SiO2 NPs with ALS and SOS, as illustrated in Fig. 3b. For all samples, IR peaks appeared at approximately 1100 cm^{-1} and 800 cm^{-1}, which are attributed to the asymmetric stretching vibrations of Si—O—Si [53]. Peaks around 470 cm^{-1} are associated with Si—O bonds [53,54]. For ALS-NPs additional absorption bands were observed at around 2950–2850 cm^{-1} and 3200–3500 cm^{-1}, attributed to C—H stretching vibrations from alkyl chains [55–57] and N—H stretching vibrations from the ammonium group (NH_4^+) in ALS [56,58], respectively. The presence of these peaks confirms the successful grafting of ALS onto the SiO_2 NPs. Furthermore, the S═O stretching vibrations observed at around 1250–1150 cm^{-1} confirm the presence of the sulfate group in ALS [59,60]. For the SOS-NPs, three key absorption bands were identified around 2950–2850 cm^{-1}, 1640–1620 cm^{-1}, and 1200 cm^{-1}. These peaks correspond to C—H stretching vibrations from alkyl chains [57], C═C stretching vibrations from olefin group [61–63], and S═O stretching vibrations [59] from the sulfonate group in SOS, respectively. The detected bands in the spectra of ALS-NPs and SOS-NPs verify the effective functionalisation of the SiO_2 NPs.

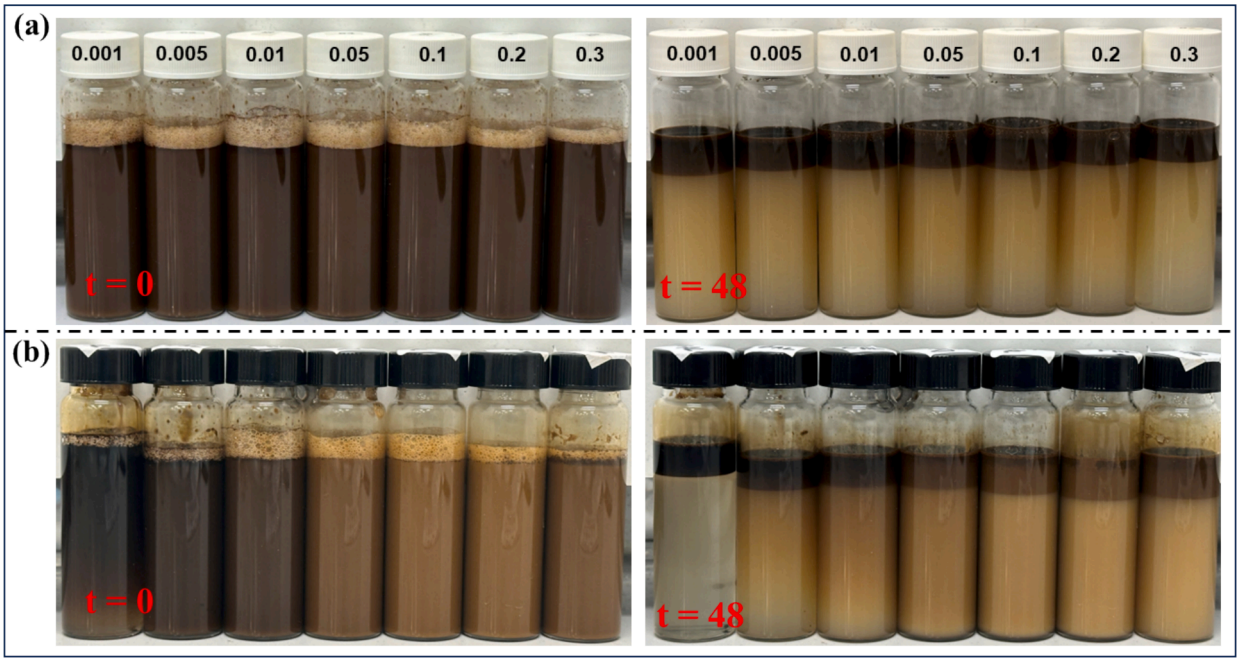

Fig. 2. Formation of oil/water emulsions using (a) ALS and (b) SOS surfactants observed over a 48-h period.

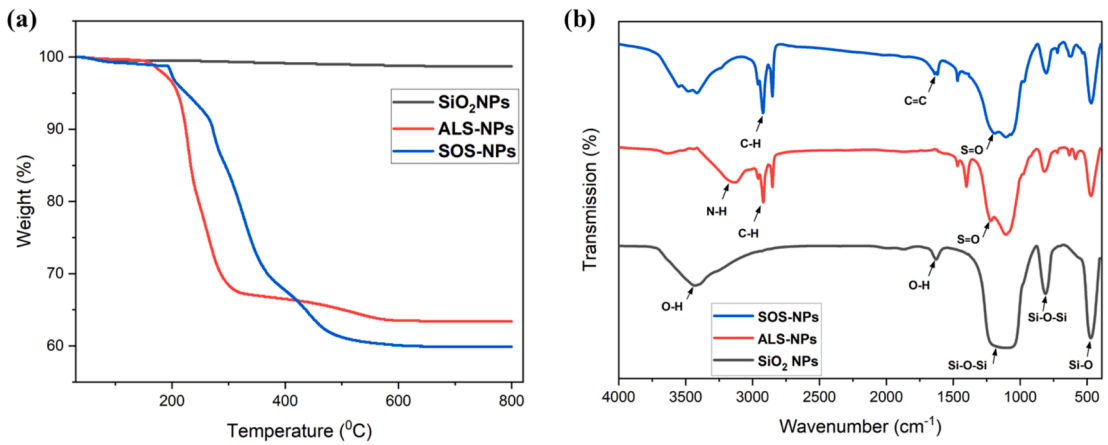

Fig. 3. (a) TGA thermograms and (b) FTIR spectroscopy in the framework regions of 400–4000 cm^{-1}, for SiO_2, ALS-NPs and SOS-NPs.

3.2.2. Surface area and morphology measurement

The textural characteristics and properties of the SiO_2 NPs, both before and after functionalisation were evaluated using the BET method. Fig. S10 presents the adsorption and desorption isotherms for SiO_2 NPs, ALS-NPs, and SOS-NPs. All isotherms resemble Type II isotherms, which are typically observed when adsorption occurs on nonporous powders or powders with pore diameters larger than micropores, such as meso- or macroporous materials [64]. The Barrett–Joyner–Halenda (BJH) method was employed to determine the pore size distribution of the nanomaterials, revealing that the major distribution lies within the meso- (between 20 and 50 Å) and macroporous (above 50 Å) regions [65]. The BET analysis indicated surface areas of 287 m^2/g for SiO_2 NPs, 105.85 m^2/g for ALS-NPs and 102.68 m^2/g for SOS-NPs. The significant reduction in the surface area for the functionalised SiO_2 NPs can be attributed to the coverage of SiO_2 NPs surfaces by ALS and SOS agents, potentially affecting the adsorption and diffusion of N_2 molecules into the internal pores. Table 2 presents the BET surface area, and particle size data for SiO_2 NPs, ALS-NPs, and SOS-NPs, including the estimated particle size from BET, particle size range from TEM, and average particle size from DLS. Assuming the particles are perfectly spherical [66], the particle size (in nm) was estimated using the equation $\mathbf{d = 6000/(S_A.\rho)}$, where $\boldsymbol{d}$ is the particle size in nm, $\boldsymbol{S_A}$ is the experimentally measured specific surface area ($m^2\ g^{-1}$), and $\boldsymbol{\rho}$ is the SiO_2 density (2.4 g cm^{-3}). The estimated particle sizes of the non-functionalised SiO_2 obtained from BET surface area, TEM and DLS tests were significantly different from those of ALS-NPs and SOS-NPs. This difference indicates that the non-functionalised SiO_2 NPs tend to agglomerate more rapidly in aqueous conditions compared to the functionalised NPs with ALS and SOS surfactants.

The morphology of the prepared NPs was examined using TEM analyses, as shown in Fig. 4, which presents images of SiO_2 NPs, ALS-NPs, and SOS-NPs. The TEM analysis revealed no significant changes in shape or size for the SiO_2 NPs before and after functionalisation with ALS and SOS. All samples exhibited a roughly spherical morphology and an average diameter of approximately 20 nm, indicating that the functionalisation process did not change the shape and the fundamental structure of the NPs. The EDX spectra results for the different prepared samples are shown in Fig. S11. These results collectively demonstrate that the procedure used to prepare ALS-NPs and SOS-NPs preserves the shape, structure, and morphology of the NP, indicating that the functionalisation process does not adversely affect these properties.

Table 2
BET surface area and particle size data for SiO_2 NPs, ALS-NPs, and SOS-NPs, including estimated particle size (BET), particle size range (TEM), and average particle size (DLS).

Sample	BET surface area (m^2g^{-1})	particle size range from TEM (nm)	estimated particle size from BET (nm)	average particle size from DLS (nm)
SiO_2 NPs	287	10–20	9	190
ALS-NPs	105.85	10–20	23.61	25
SOS-NPs	102.68	10–20	24.35	15

3.3. Characterisation of nanofluids

3.3.1. IFT measurement

The IFT measurements illustrated in Fig. 5 provide comprehensive comparison of the efficacy of various nanofluid formulations in reducing IFT. Fig. 5a shows the IFT measurements of virgin SiO_2 NPs, which maintain a relatively high and stable IFT values across different concentrations and over time, indicating limited effectiveness in reducing IFT. By contrast, Fig. 5b and d show the performance of ALS and SOS surfactants alone, respectively. Both surfactants significantly decrease IFT at higher concentrations, demonstrating strong surface activity. Fig. 5c and e presents the IFT results for the modified SiO_2 NPs with ALS and SOS surfactants (ALS-NPs and SOS-NPs). The functionalised SiO_2 NPs show a further reduction in IFT compared to both virgin SiO_2 NPs and the surfactants alone. For instance, 100 ppm of ALS-NPs, which contains around 34 ppm of ALS based on TGA-analyses, achieved an IFT reduction approximately 10 times lower than 100 ppm and 5 times lower than 500 ppm of ALS alone. Similarly, 100 ppm of SOS-NPs, containing around 37.5 ppm of SOS, showed a significant IFT reduction compared to 100 ppm and 500 ppm of SOS. These results indicated that grafting the SiO_2 NPs with ALS and SOS surfactants not only significantly reduced the IFT but also decreased the amount of surfactant required.

All the measurements were conducted without the addition of alkali due to instrument limitations, as the device was unable to measure extremely low IFT values. Upon introducing 0.1 wt% alkali to 100 ppm SOS-S NPs, the oil droplet failed to form, suggesting an IFT within the range of 10^{-2}–10^{-4} mN/m. This significant reduction in IFT highlights the formation of a stable interfacial film.

This grafting approach effectively achieved ultra-low IFT values at low surfactant concentrations, thereby minimising chemical consumption and enhancing both cost efficiency and environmental sustainability. These attributes are essential for the practical implementation of EOR applications.

3.3.2. Zeta potential measurements and size distribution

NPs often exhibit a tendency to aggregate due to the attractive forces between them, which can diminish their stability and negatively impact

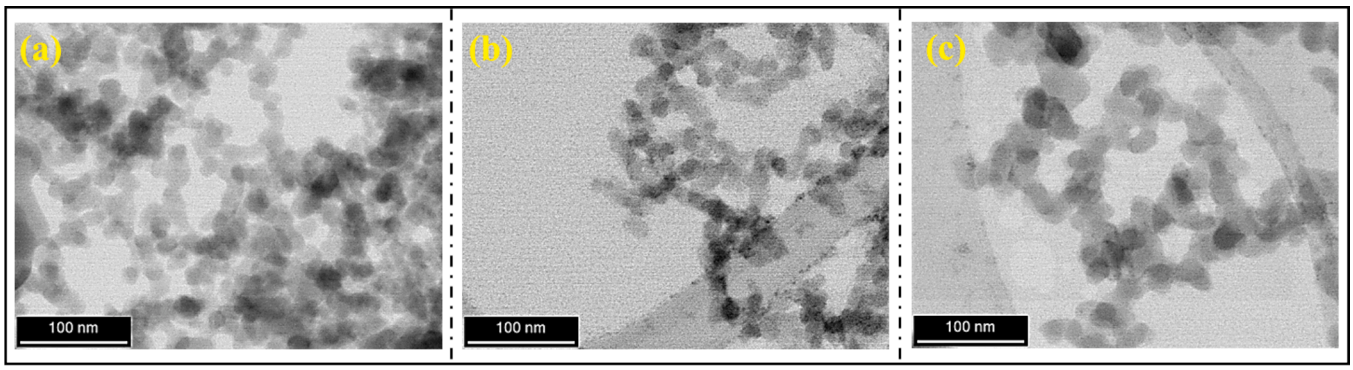

Fig. 4. TEM images for (a) the unmodified SiO_2 NPs, (b) ALS-NPs, and (c) SOS-NPs.

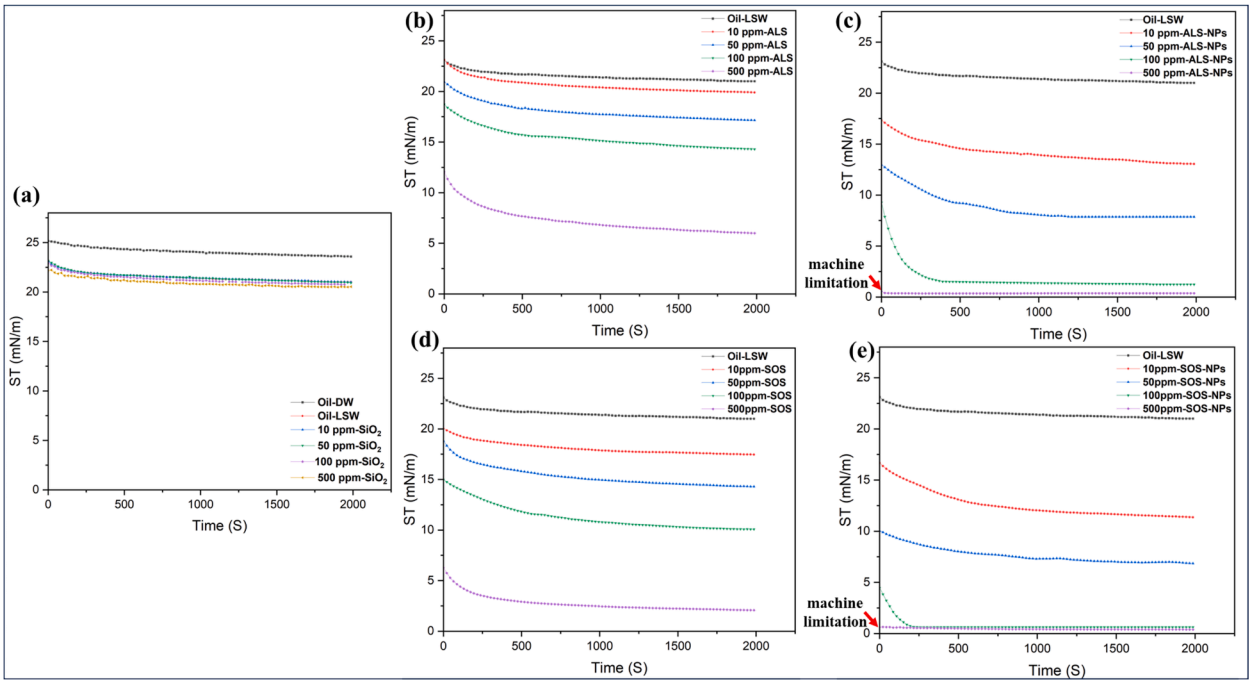

Fig. 5. IFT measurement between crude oil droplet and different surfactants and nanofluids over time with concentrations ranging from 0 to 500 ppm, (a) unmodified SiO_2 NPs, (b) ALS alone, (c) SOS alone, (d) ALS-NPs, and (e) SOS-NPs.

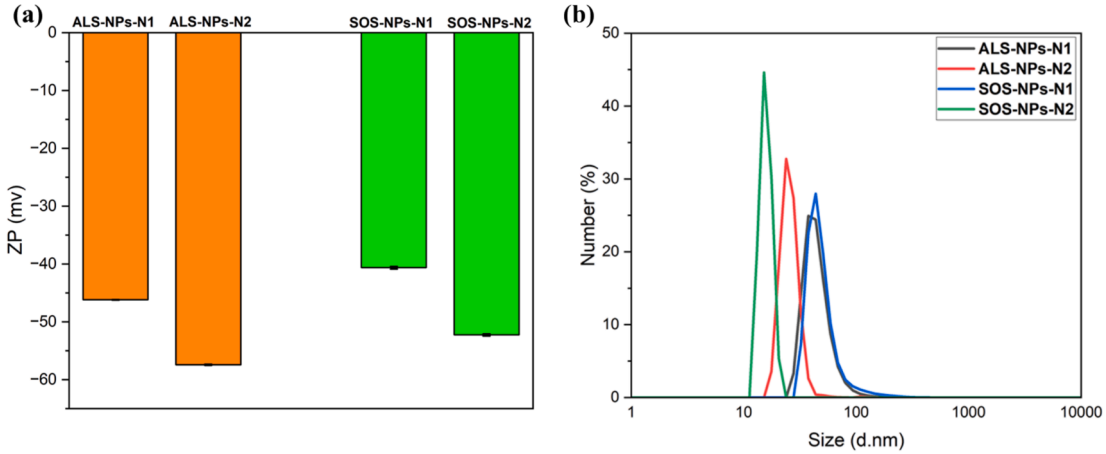

Fig. 6. (a) ZP and (b) the DLS analyses of ALS-NPs and SOS-NPs without (N1) and the with alkali (N2).

their performance in EOR applications [67]. To mitigate this issue, surface modification of NPs with surfactants can prevent aggregation. ZP is a critical parameter for determining the surface charge and stability of NPs. NPs with highly positive or negative ZP values (ZP >+30 mV; ZP < −30 mV) exhibit strong electrostatic repulsion, which enhances stability and minimises aggregation and precipitation. In contrast, NPs with low ZP values (−30 < ZP < +30 mV) are prone to aggregation due to the increased attractive forces, leading to instability [68].

The ZP results indicate that grafting SiO_2 NPs with ALS and SOS surfactants significantly increased their ZP values to approximately −46 mV and −40 mV, respectively, demonstrated enhanced stability (see Fig. 6a and Fig. S12). To evaluate their stability at elevated temperatures, ZP measurements were conducted at 60 °C. For ALS-NPs, the ZP was approximately −43 mV, while for SOS-NPs, it was around −38 mV. These results confirm the stability of the prepared nanofluids at high temperatures (see Fig. S13).

Additional ZP measurements were conducted at a concentration of 100 ppm for both ALS-NPs and SOS-NPs before (N1) and after (N2) the addition of 0.1 wt% alkali in order to further investigate the impact of alkali on nanofluid stability. As shown in Fig. 6a, the addition of alkali increased the ZP by approximately −10 mV for both nanofluids, suggesting enhanced stability due to increased electrostatic repulsion. The size distribution measurements further confirmed the stabilising effect of surfactant modification, with particle sizes of SiO_2 NPs decreasing significantly after modification with ALS and SOS surfactant to around 45 and 51 nm, respectively (see Fig. 6b and Fig. S12). Moreover, the addition of alkali further decreased the particle sizes of ALS-NPs and SOS-NPs to around 25 and 15 nm, respectively, as shown in Fig. 6b. These findings highlight the role of alkali in further enhancing the stability of the NPs.

3.4. Characterisation studies for nanoemulsions

3.4.1. Investigating emulsion stability for optimal nanofluid performance

For the EOR applications, various tests were conducted to screen and optimise various concentrations of ALS-NPs and SOS-NPs, using a selected oil–water ratio and alkali concentration. The objective was to determine the most effective nanofluid concentration based on its ability to spontaneously form emulsions in situ. Fig. 7 demonstrates the spontaneously emulsified ALS-NPs and SOS-NPs immediately after preparation and following two weeks of aging, respectively. It is important to note that all emulsions were formed spontaneously without the application of shear force, requiring only gentle flipping. Upon visual inspection, the samples prepared with ALS-NPs and SOS-NPs showed greater stability over a two-week aging period compared to those prepared with ALS and SOS surfactants alone (see Fig. 2). The most stable emulsions were observed at a concentration of 100 ppm for both ALS-NPs and SOS-NPs.

At higher concentrations, some limitations were observed. For ALS-NPs, samples with concentrations of 2000 ppm and above exhibited noticeable NPs settling at the bottom of the vials. Similarly, SOS-NPs showed aggregation at concentrations exceeding 500 ppm. This aggregation is attributed to the dominance of intermolecular interactions, such as van der Waals forces, over stabilizing forces like the electrostatic repulsion provided by the surfactants [69]. When the concentration of NPs surpasses a critical threshold, these destabilising interactions hinder the uniform dispersion of NPs in the fluid, reducing emulsion stability.

The CD % was also used to quantify the effect of concentration on the emulsion stability with ALS-NPs and SOS-NPs, as well as for ALS and SOS surfactants alone. Fig. 8a and b show the CD % for different concentrations after two-week aging period. The results indicate that grafting SiO_2 with both surfactants significantly reduced the CD % compared to the surfactants alone, thereby confirming the positive impact of grafting on oil/water emulsion stability. Among the tested concentrations, ALS-NPs and SOS-NPs exhibited the highest emulsion stability, with lowest CD % observed at 100 ppm. Therefore, this concentration was selected for further investigations.

3.4.2. Droplet size distribution of spontaneous emulsion

Spontaneous emulsification in porous media is essential for effective fluid flow at the pore level, making it an effective method for EOR during chemical flooding. Emulsions with smaller droplet sizes are particularly desirable, as these can easily penetrate micropores, thereby improving sweep and displacement efficiency [16,70]. In this work the spontaneous emulsions formulated by ALS-NPs and SOS-NPs were analysed using particle size analyses. Fig. 9 shows the average droplet size distribution of emulsions formed in the presence of 100 ppm of ALS or SOS alone compared to ALS-NPs and SOS-NPs (without alkali). Due to the dilution required for MasterSizer analysis, conclusive size distribution measurements could not be obtained for ALS and SOS with alkali. As result, only the droplet size measurements obtained through image

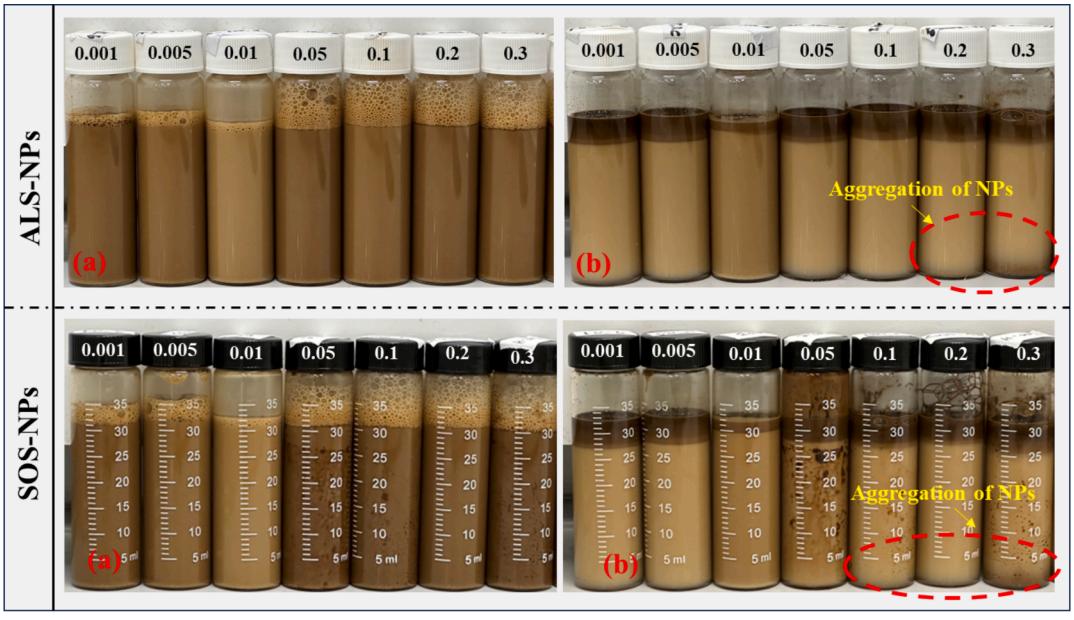

Fig. 7. Spontaneous emulsification of different ALS-NPs and SOS-NPs concentrations, (a) initially and (b) after two weeks.

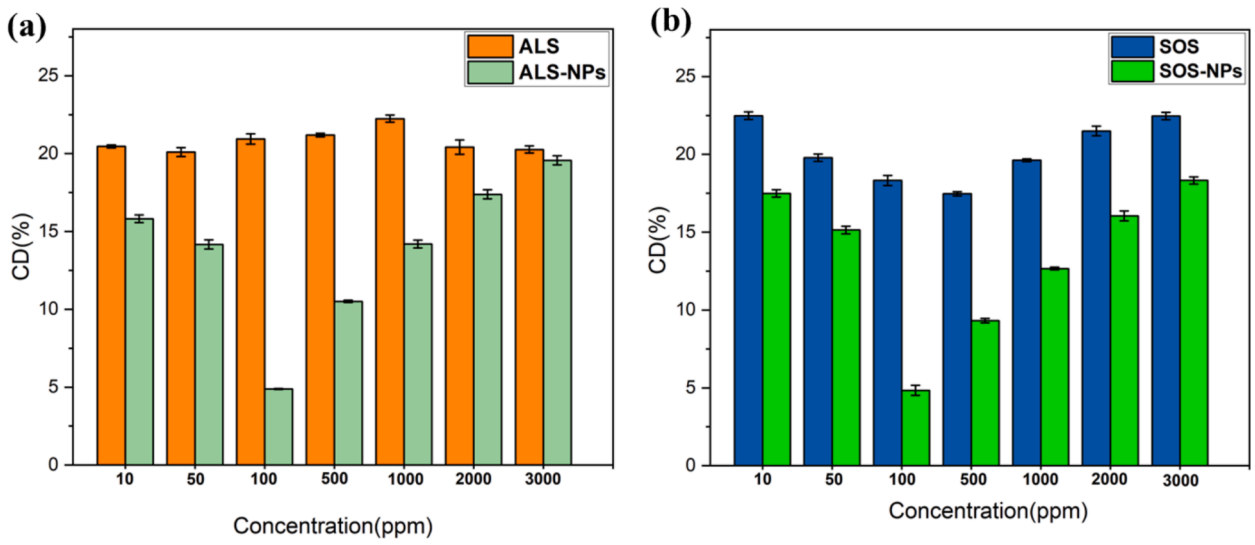

Fig. 8. The creaming degree (CD %) of emulsions stabilised by (a) ALS and ALS-NPs, (b) SOS and SOS-NPs at different concentrations after two weeks.

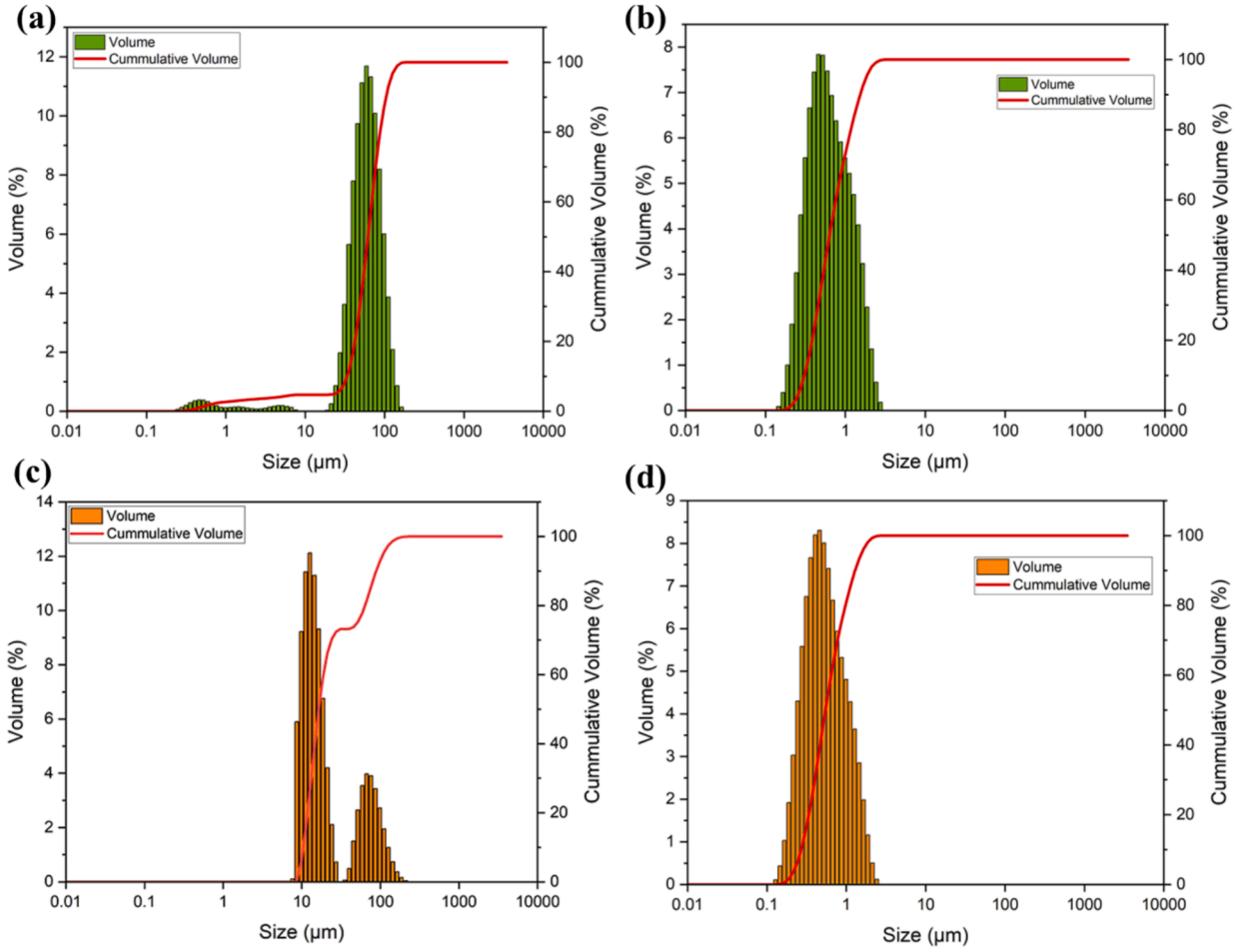

Fig. 9. The average droplet size distribution of emulsions formed in the presence of 100 ppm of (a) ALS, (c) SOS alone, compared to (b) ALS-NPs and (d) SOS-NPs.

analysis are reported, as illustrated later in Fig. 10. It is evident from the MasterSizer results that the size distribution of the oil droplets significantly decreased when ALS-NPs and SOS-NPs were used, compared to ALS or SOS alone (without alkali). The spontaneously generated emulsions with grafted SiO_2 NPs showed a notable shift towards smaller droplet sizes. Using surfactant alone might create injection problems due to larger droplet sizes, especially in reservoirs with small pore sizes [15]. However, the droplet size formed in the presence ALS-NPs and SOS-NPs were small enough to penetrate the pores, thus improving microscopic sweep efficiency in the reservoirs. This improvement is attributed to the role of NPs as nanocarriers for surfactants, facilitating the formation of stable emulsifications with smaller droplet size

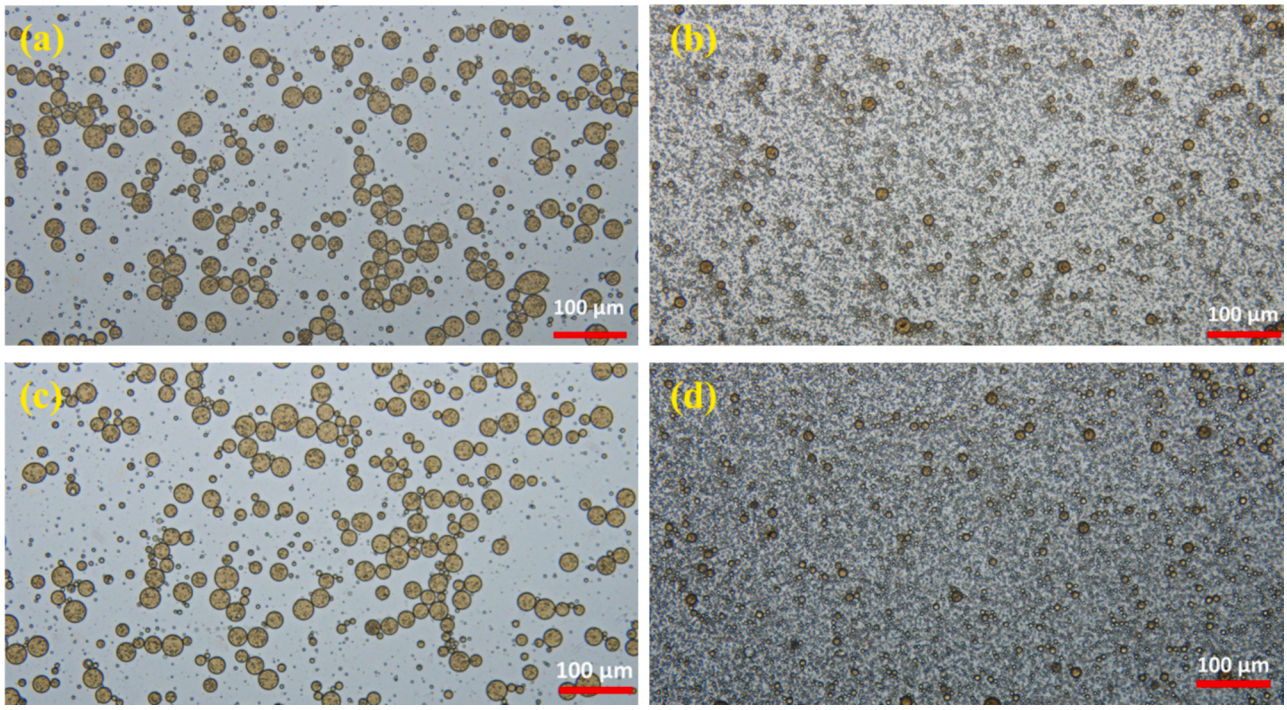

Fig. 10. Microscopic images of the oil droplets generated using (a) ALS, (b) ALS-NPs, (c) SOS, and (d) SOS-NPs.

distributions.

For further investigation, microscopic imaging was conducted on the prepared emulsions. Fig. S14 shows the oil droplets generated using ALS and SOS surfactants alone, without the addition of alkali. The observed droplet sizes align with the result shown in Fig. 9a, and c. Fig. 10 displays the oil droplets when alkali was added: Fig. 10a and b show results for ALS and ALS-NPS, while Fig. 10c and d present results for SOS and SOS-NPs. The images show that after the inclusion of alkali, the oil droplets-size reduced slightly. However, smaller droplets generated using ALS-NPs and SOS-NPs compared to those formulated with the surfactants alone. It is worth pointing that a few relatively larger droplets (10–20 µm) were observed for ALS-NPs and SOS-NPs under microscopic analysis, which were not evident in the MasterSizer analysis. This could be due to the differences in sample preparation for the two techniques and the dilution step required for MasterSizer measurement. Consequently, a concentration of 100 ppm for both ALS-NPs and SOS-NPs was selected for EOR applications, including spontaneous imbibition and micromodel flooding test.

3.5. EOR evaluation

3.5.1. Contact angle measurement

Contact angle measurement is a critical quantitative method for evaluating surface wettability. Reservoirs are typically water-wet by nature; however, they can become oil-wet due to the accumulation of heavier hydrocarbons on the rock surface. Wettability is classified based on the three-phase contact angle: water-wet, with angles ranging from 0° to 75°; intermediate-wet, between 75° and 105°; and oil-wet, from 105° to 180°, with measurements referenced to the denser phase [71]. This study aims to investigate the potential of nanofluids to alter rock surface wettability towards a water-wet state. Contact angle measurements were taken relative to the less dense phase, with values greater than 90° indicating water-wetness and those below 90° signifying oil-wetness. Fig. S15 presents the contact angle measurements obtained both before and after the aging process, as also reported in our previous study [35]. The results demonstrate that aging significantly altered the wettability of the standard substrate from water-wet to strongly oil-wet. This change can be attributed to the partial adsorption of polar components from the crude oil onto the sandstone surface. Fig. 11 shows the contact angle measurement of oil droplet at the three-phase oil-fluid-rock interface at room temperature, using different surfactants and nanofluids. The estimated contact angles were around 105° and 120° for ALS and SOS surfactants alone, respectively. In contrast, the contact angles observed were around 76°, 161° and 176° for SiO_2 NPs, ALS-NPs, and SOS-NPs, respectively. Therefore, the use of surfactants alone shifted the rock wettability to intermediate wet, while SiO_2 NPs alone produced only slightly increase in the contact angle, highlighting their limitations in altering rock surface wettability. Notably, the presence of ALS-NPS and SOS-NPs significantly changed the wettability of the rock from oil-wet to strongly water wet. This finding demonstrates the effectiveness of functionalised SiO_2 NPs with ALS and SOS surfactants in achieving desirable wettability alteration in reservoir rocks. This approach can play a significant role in EOR applications compared to using SiO_2 NPs or surfactants alone.

3.5.2. EOR by spontaneous imbibition test

The spontaneous imbibition tests were conducted on saturated oil-wet Berea sandstone cores using different fluids over a twenty-day period (Fig. S16). The effectiveness of different prepared fluids, both with and without NPs in EOR was systematically carried out through these tests. The recovery performance of each fluid was analysed based on their different characteristics and interactions with the core materials, highlighting the impact of these fluids on oil displacement efficiency. As shown in Fig. 12, the use of non-modified SiO_2 NPs resulted in the lowest oil recovery, at around 27 % of the OOIP, reaching a plateau on Day 5. This poor performance is likely due to the lower wettability alteration and potential aggregation of the SiO_2 NPs, which could lead to pore blockage within the cores. The lack of stability of SiO_2 NPs dispersion reduced their effectiveness, as agglomerated particles hindered the flow pathways necessary for efficient oil displacement. In contrast, ALS and SOS surfactants alone exhibited improved oil recovery compared to SiO_2 NPs alone, with SOS achieving approximately 44 % recovery and ALS around 42 %, reaching plateaus on days 8 and 7, respectively. This improved performance can be attributed to the

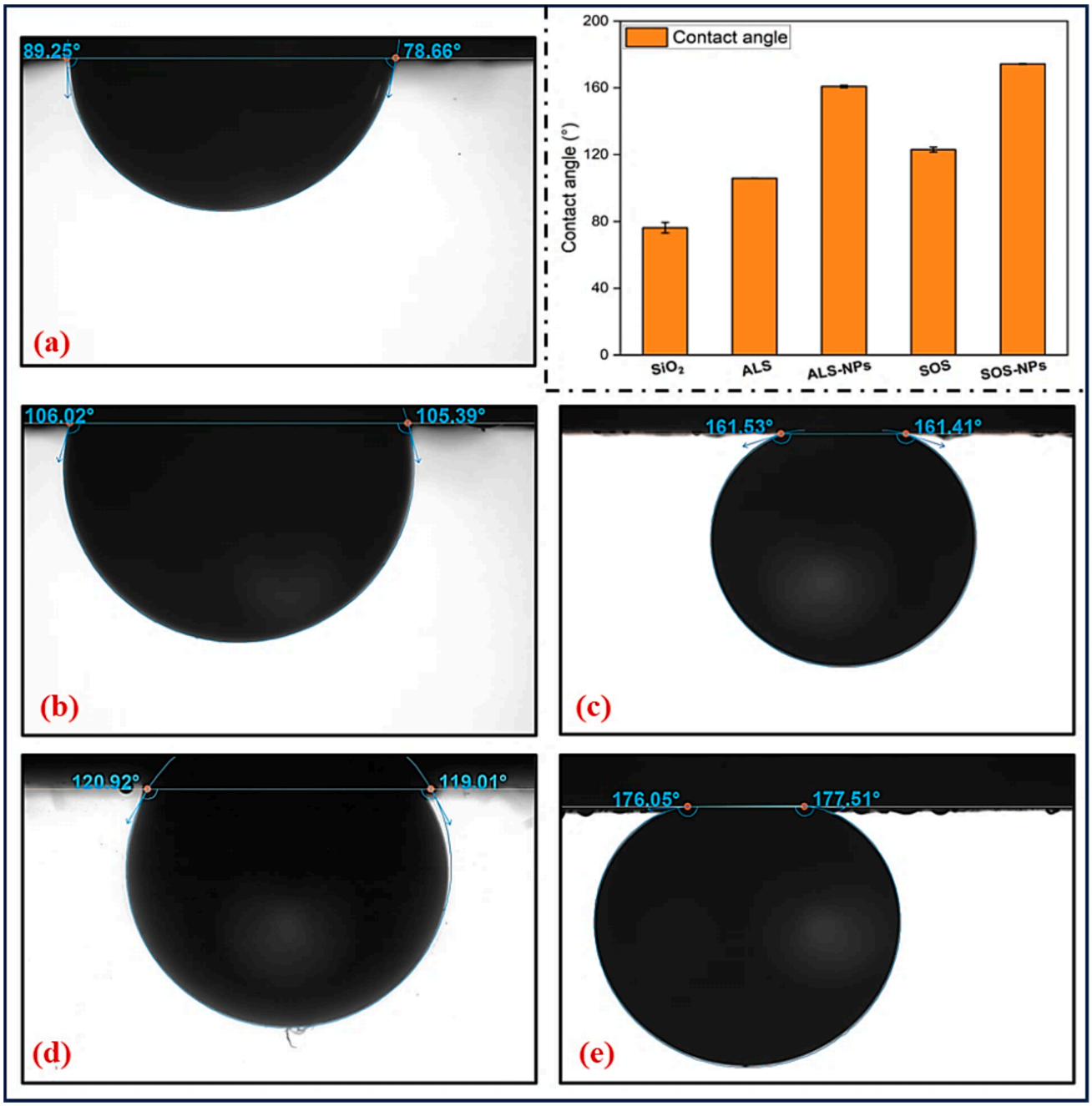

Fig. 11. Contact angle measurement in the presence of (a) SiO_2 NPs, (b) ALS, (c) ALS-NPs, (d) SOS, and (e) SOS-NPs.

surfactants' ability to alter rock surface wettability from oil-wet to water-wet through adsorption onto the core surface, facilitating better displacement of oil by water.

Functionalising the SiO_2 NPs with ALS and SOS surfactants achieved the highest oil recovery rates. The SOS-NPs showed the most substantial oil recovery at around 70 %, while ALS-NPs recovered about 66 %, reaching plateaus after around 12 days, and 10 days, respectively. This significant improvement is attributed to the combined effects of wettability alteration and the formation of spontaneous emulsions. Functionalised NPs not only improved the wettability alteration, as evidenced by contact angle measurements, but also facilitated the formation of smaller and more stable oil in water emulsions. The smaller and more stable oil droplets created by ALS-NPs and SOS-NPs enhanced the mobilisation and recovery of oil, as these smaller droplets could more easily displace through the pore network of the core, reducing the possibility of blockage. This dual action enhanced the overall displacement efficiency and contributed to the higher recovery rates observed. As illustrated in Fig. S17, the oil droplets on the surface of the cores treated with surfactants alone were significantly larger compared to those treated with SOS-NPs and ALS-NPs. This observation highlights the higher stability and dispersibility of the functionalised SiO_2 NPs dispersions, which are important for achieving higher oil recovery performance. Additionally, functionalising the SiO_2 NPs with these surfactants led to a reduction in the required concentration of surfactants compared to using the surfactants alone. These synergistic effects not only improve oil recovery but also reduced surfactant consumption, enhancing the cost effectiveness of the process. Fig. S18 illustrates the difference in colour between the different core samples after the imbibition tests. The cores imbibed with SiO_2 NPs, ALS, and SOS individually exhibited a darker brown colour, whereas the cores saturated with ALS-

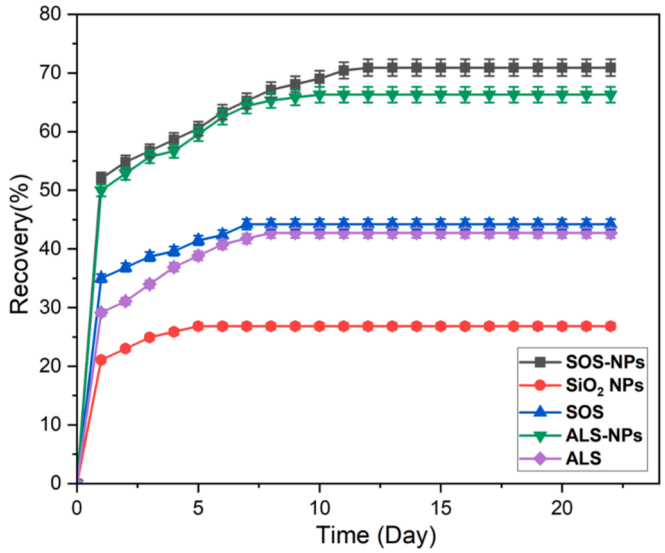

Fig. 12. Oil recovery during spontaneous imbibition test using different prepared fluids.

NPs and SOS-NPs displayed a lighter colour. This observation aligns with the results obtained from the imbibition test.

To validate the stability of the prepared nanofluids under reservoir-like conditions, additional experiments were performed. ALS-NPs and SOS-NPs were suspended in aqueous solutions with a Berea sandstone core under the same conditions as the imbibition tests. The suspensions were aged for 10 days (ALS-NPs) and 12 days (SOS-NPs), corresponding to the time required to reach maximum EOR, as shown in Fig. 12. After aging, the samples were sonicated for 15 min and centrifuged to remove detached surfactants. The NPs were then isolated, washed, and analysed via TGA.

Fig. S19 shows the TGA results of the aged NPs, which revealed no significant changes in weight loss compared to the original TGA results obtained before the imbibition tests. The weight loss remained approximately 2 % for both ALS-NPs and SOS-NPs, confirming that the surfactants remained strongly attached to the NPs even after prolonged exposure to reservoir-like conditions.

3.5.3. Oil recovery by micromodel flooding test

The micromodel flooding tests on oil-wet microchips provided valuable insights into the fluid flow dynamics within porous media and the effectiveness of different nanofluids in EOR. These flooding tests involved sequential flooding with LSW for secondary oil recovery, followed by the injection of different surfactants and nonfluids. The resulting tertiary oil recovery rates over time for the differently prepared samples are illustrated in Fig. 13. The non functionalised SiO_2 NPs showed the lowest recovery rate, around 6 %. This low recovery rate may be due to the poor wettability alteration and possible aggregation of non-modified SiO_2 NPs, preventing efficient oil displacement. However, for the ALS and SOS surfactant flooding, the recovery rate quickly reached approximately 38 % and remained constant. This performance indicates that both SOS and ALS surfactants alone can significantly alter the wettability of the oil-wet microchip, thereby improving oil recovery. For ALS-NPs and SOS-NPs, the recovery rate increased significantly over the first few hours, gradually plateauing at around 74 % for ALS-NPs and approximately 80 % for SOS-NPs. The obtained high oil recovery can be attributed to the synergistic effects of wettability alteration and spontaneous emulsification. The grafting of the SiO_2 NPs with these two surfactants enhanced the interaction between the NPs and the oil-wet surface. This enhancement resulted in the formation of small oil droplets that were easily displaced through the porous system, compared to the larger droplets created during surfactant flooding (see Fig. 14). This improvement is illustrated by an approximately increase of oil recovery by 36 % with ALS-NPs and 42 % with SOS-NPs compared to surfactants flooding alone. Table S2 shows the videos of the microchips during the flooding tests conducted with various prepared fluids and nanofluids, observed and monitored over a duration of 10 h.

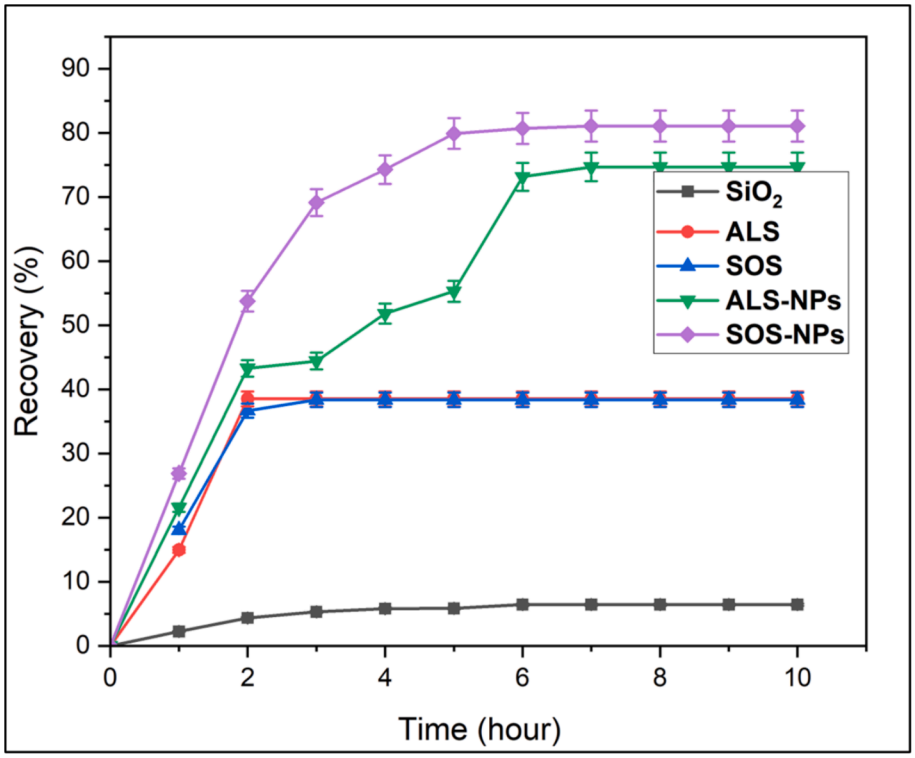

Fig. 13. Tertiary oil recovery rates over time as determined through microfluidic flooding tests for the different prepared samples.

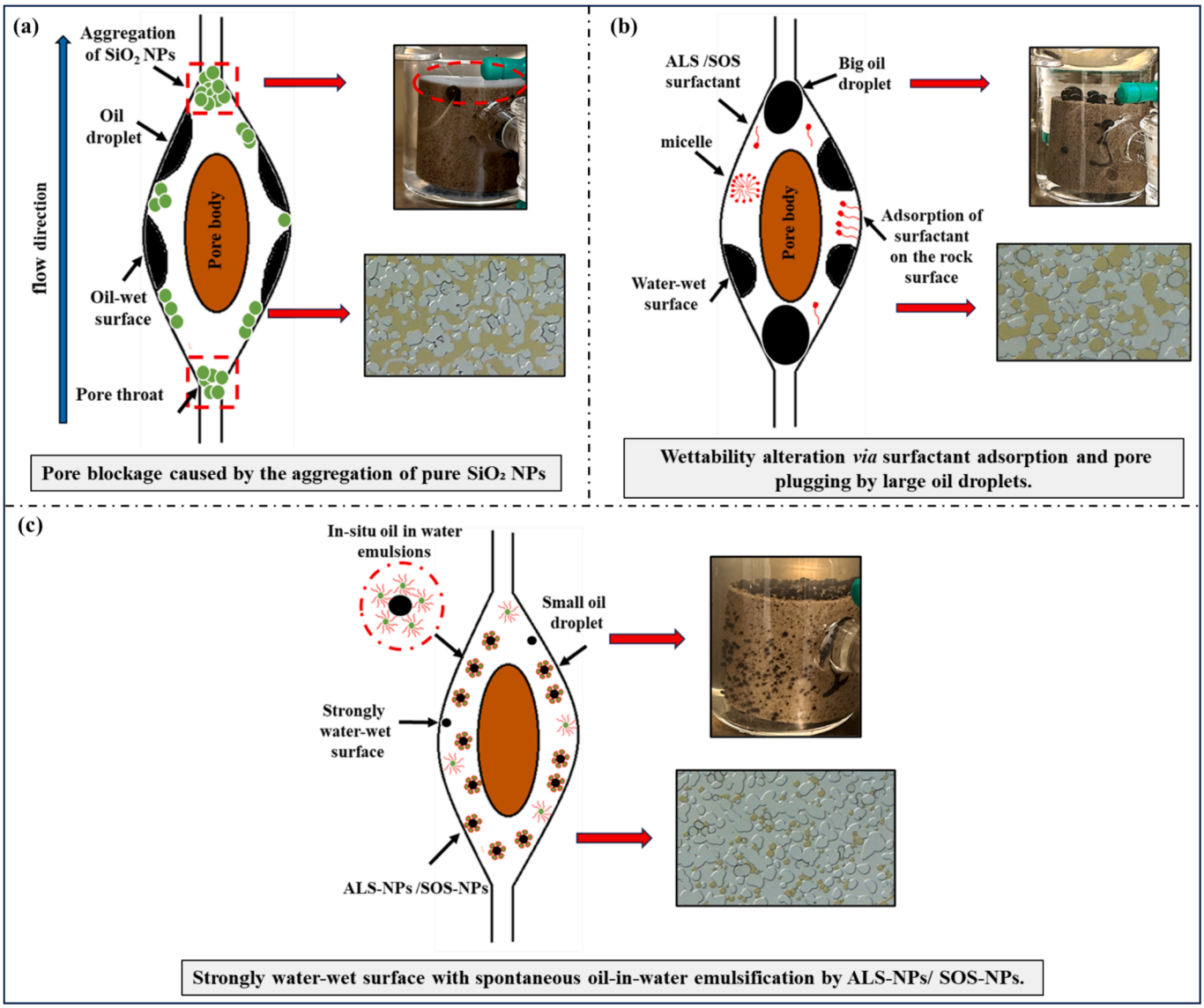

Fig. 14. Proposed mechanisms for EOR using (a) SiO_2 NPs, (b) surfactants alone, and (c) modified SiO_2 with surfactants.

3.5.4. Mechanisms and efficacy of ALS and SOS-NPs nanofluids for EOR in oil-wet porous media

Emulsion blockage in porous media can be classified into different types based on the relative diameter of the emulsions and the pores, including plugging by single droplets [72]. Notably, while ALS and SOS used for imbibition test and microfluidic flooding tests have effectively altered rock wettability and enhanced oil recovery compared to non-functionalised SiO_2 NPs, they have resulted in larger oil droplets, which may block pores. Fig. 14 shows the suggested mechanism by which ALS and SOS grafted SiO_2 nanofluids mobilised trapped oil when injected into oil-wet sandstone porous media. The dual affinity of the ALS-NPs and SOS-NPs nanofluids for both water and oil facilitated the in-situ formation of stable emulsions, enhancing interactions with crude oil. This interaction significantly altered the rock wettability (as demonstrated by contact angle measurements), formed smaller emulsion droplets, and reduced the IFT. Additionally, the alkaline environment further stabilised the nanofluids and contributed to further IFT reduction. The formation of smaller emulsion droplets increases the contact area between the oil and the rock, facilitating more effective mobilization of the trapped oil [73,74]. These smaller droplets are capable of penetrating deeper into the rock matrix, displacing a greater volume of oil and minimising the probability of oil entrapment [16,73], as illustrated in Fig. 14c. It is important to note that, while the prepared nanofluids enhanced oil recovery, the efficacy of these mechanisms is influenced by multiple factors, including the type of the crude oil, the specific characteristic of the nanofluids (such as stability), and reservoir properties [16,74,75]. In summary, the use of ALS-NPs and SOS-NPs nanofluids presented a promising method for EOR by altering rock wettability, reducing IFT, stabilising oil in water emulsions, and facilitating deeper penetration and mobilisation of trapped oil. However, further investigations on core flooding tests in different reservoir conditions and field-scale testing are essential to validate and optimise these approaches for future applications.

4. Conclusion

This study investigated the application of functionalised SiO_2 NPs for EOR. The SiO_2 NPs were surface modified with two selected surfactants, ALS and SOS, under optimal conditions and without the use of binding agents. This research represents the first application of these functionalised NPs in EOR. The findings demonstrate the considerable potential of functionalised SiO_2 NPs to enhance oil recovery by altering rock wettability, reducing IFT, and forming stable oil-in-water emulsions. These mechanisms facilitated the deeper penetration and mobilisation

of trapped oil within porous media.

Microfluidic and spontaneous imbibition experiments revealed that ALS-NPs and SOS-NPs outperformed traditional surfactants and non-functionalised SiO_2 NPs, achieving significantly higher oil recovery rates. The dual affinity of these functionalised NPs for both water and oil enabled the spontaneous formation of smaller and more stable emulsion droplets, enhancing displacement efficiency and reducing the likelihood of pore blockage. Furthermore, the stability of these nanofluids was improved under alkaline conditions, contributing to a greater reduction in IFT.

This study underscores the importance of NPs-surfactant synergy in optimising EOR processes. The use of grafted SiO_2 NPs proved effective in reducing the required concentrations of surfactants, thereby making the process more cost-effective and potentially scalable for field applications. However, the effectiveness of these nanofluids is influenced by several factors, including the type of crude oil and reservoir properties. Further investigations and field-scale testing are therefore required to validate and optimise these approaches for practical EOR applications.

CRediT authorship contribution statement

Louey Tliba: Writing – review & editing, Writing – original draft, Methodology, Investigation, Formal analysis, Data curation, Conceptualization, Validation. **Mohamed Edokali:** Writing – review & editing, Investigation, Formal analysis. **Thomas Moore:** Resources. **Omar Choudhry:** Software. **Paul W.J. Glover:** Writing – review & editing, Supervision, Data curation. **Robert Menzel:** Writing – review & editing, Supervision, Methodology, Investigation, Formal analysis. **Ali Hassanpour:** Writing – review & editing, Supervision, Methodology, Investigation, Formal analysis, Conceptualization.

Declaration of competing interest

The authors declare that they have no known competing financial interests or personal relationships that could have appeared to influence the work reported in this paper.

Acknowledgement

The authors would like to extend their sincere gratitude to the following individuals for their significant contributions: Dr. Ben Douglas, Dr. Adrian Cunliffe, and Dr. Karine Alves Thorne from school of chemical and process engineering; Dr. Zabeada Aslam and Mr. Stuart Micklethwaite and from the Leeds Electron microscopy and spectroscopy centre (LEMAS); and Dr. Farad Sagala, and Dr. Afif Hethnawi from University of Calgary. Special thanks are given to Mr. John Wyn Williams from the School of Earth and Environment at the University of Leeds for his invaluable assistance with sample preparation.

Appendix A. Supplementary material

Supplementary data to this article can be found online at https://doi.org/10.1016/j.molliq.2025.127021.

Data availability

Data will be made available on request.

References

[1] (EIA), T.U.S.E.I.A., International Energy Outlook 2023, 2023.
[2] X. Zhong, et al., Increased nonionic surfactant efficiency in oil recovery by integrating with hydrophilic silica nanoparticle, Energy Fuel 33 (9) (2019) 8522–8529.
[3] A. Agi, et al., Natural polymer flow behaviour in porous media for enhanced oil recovery applications: a review, J. Pet. Explor. Prod. Technol. 8 (2018) 1349–1362.
[4] A.O. Gbadamosi, et al., An overview of chemical enhanced oil recovery: recent advances and prospects, Int. Nano Lett. 9 (2019) 171–202.
[5] S. Park, E.S. Lee, W.R.W. Sulaiman, Adsorption behaviors of surfactants for chemical flooding in enhanced oil recovery, J. Ind. Eng. Chem. 21 (2015) 1239–1245.
[6] M. El-Dairi, R.J. House, Optic nerve hypoplasia, in: Handbook of Pediatric Retinal OCT and the Eye-Brain Connection, Elsevier, 2020, pp. 285–287.
[7] P. Druetta, P. Raffa, F. Picchioni, Chemical enhanced oil recovery and the role of chemical product design, Appl. Energy 252 (2019) 113480.
[8] R. Ganjdanesh et al., A field pilot of huff-n-puff gas injection for enhanced oil recovery in Permian Basin, in: SPE Annual Technical Conference and Exhibition, OnePetro, 2020.
[9] O. Massarweh, A.S. Abushaikha, The use of surfactants in enhanced oil recovery: a review of recent advances, Energy Rep. 6 (2020) 3150–3178.
[10] C. Negin, S. Ali, Q. Xie, Most common surfactants employed in chemical enhanced oil recovery, Petroleum 3 (2) (2017) 197–211.
[11] D. Langevin, D. Langevin, Emulsions and Foams, Springer, 2020.
[12] Z. Li, et al., Fabrication and mechanism study of the fast spontaneous emulsification of crude oil with anionic/cationic surfactants as an enhanced oil recovery (EOR) method for low-permeability reservoirs, Energy Fuel 33 (9) (2019) 8279–8288.
[13] J. Song, et al., Evaluating physicochemical properties of crude oil as indicators of low-salinity–induced wettability alteration in carbonate minerals, Sci. Rep. 10 (1) (2020) 3762.
[14] M. Tagavifar, et al., Spontaneous and flow-driven interfacial phase change: dynamics of microemulsion formation at the pore scale, Langmuir 33 (45) (2017) 13077–13086.
[15] A. Hethnawi, et al., Influence of CTAB-grafted faujasite nanoparticles on the dynamic interfacial tension of oil/water systems, Energy Fuel 36 (11) (2022) 5666–5680.
[16] F. Sagala, et al., Formulation of spontaneous in situ emulsification using sodium lauryl sulfate grafted nanopyroxene for enhanced heavy oil recovery in sandstone reservoirs, Energy Fuel 37 (17) (2023) 12838–12853.
[17] M.J. Qazi, et al., Dynamic surface tension of surfactants in the presence of high salt concentrations, Langmuir 36 (27) (2020) 7956–7964.
[18] W. Yu, H. Xie, A review on nanofluids: preparation, stability mechanisms, and applications, J. Nanomater. 2012 (2012) 1–17.
[19] Y. Zhou, et al., Surfactant-augmented functional silica nanoparticle based nanofluid for enhanced oil recovery at high temperature and salinity, ACS Appl. Mater. Interfaces 11 (49) (2019) 45763–45775.
[20] N.N. Nassar, A. Ringsred, Rapid adsorption of methylene blue from aqueous solutions by goethite nanoadsorbents, Environ. Eng. Sci. 29 (8) (2012) 790–797.
[21] Y. Zhou, et al., Polymer nanoparticles based nano-fluid for enhanced oil recovery at harsh formation conditions, Fuel 267 (2020) 117251.
[22] A. Hethnawi, et al., Enhancing Chromium (VI) removal from synthetic and real tannery effluents by using diatomite-embedded nanopyroxene, Chemosphere 252 (2020) 126523.
[23] H. ShamsiJazeyi, R. Verduzco, G.J. Hirasaki, Reducing adsorption of anionic surfactant for enhanced oil recovery: Part I. Competitive adsorption mechanism, Colloids Surf. A: Physicochem. Eng. Asp. 453 (2014) 162–167.
[24] M.S. Kamal, I.A. Hussein, A.S. Sultan, Review on surfactant flooding: phase behavior, retention, IFT, and field applications, Energy Fuel 31 (8) (2017) 7701–7720.
[25] S. Maaref, A. Kantzas, S.L. Bryant, The effect of silanization assisted nanoparticle hydrophobicity on emulsion stability through droplet size distribution analysis, Chem. Eng. Sci. 201 (2019) 175–190.
[26] J. Tang, P.J. Quinlan, K.C. Tam, Stimuli-responsive Pickering emulsions: recent advances and potential applications, Soft Matter 11 (18) (2015) 3512–3529.
[27] Y. Kazemzadeh, et al., Review on application of nanoparticles for EOR purposes: a critical review of the opportunities and challenges, Chin. J. Chem. Eng. 27 (2) (2019) 237–246.
[28] W. Wang, et al., Synergistic effects of weak alkaline–surfactant–polymer and SiO2 nanoparticles flooding on enhanced heavy oil recovery, Energy Fuel 36 (14) (2022) 7402–7413.
[29] K.K. Ihekoronye, Formulation of bio-surfactant augmented with nanoparticles for enhanced oil recovery, in: SPE Nigeria Annual International Conference and Exhibition, SPE, 2022.
[30] A. Rezaei, et al., Insights into the effects of pore size distribution on the flowing behavior of carbonate rocks: linking a nano-based enhanced oil recovery method to rock typing, Nanomaterials 10 (5) (2020) 972.
[31] M. Zhao, et al., Study on the main factors and mechanism of functional silica nanofluid spontaneous imbibition for enhanced oil recovery, J. Mol. Liq. 394 (2024) 123699.
[32] G. Kumar, et al., Engineering the wettability alteration of sandstone using surfactant-assisted functional silica nanofluids in low-salinity seawater for enhanced oil recovery, ACS Eng. Au 2 (5) (2022) 421–435.
[33] P.I. Sagbana, A.S. Abushaikha, A comprehensive review of the chemical-based conformance control methods in oil reservoirs, J. Pet. Explor. Prod. Technol. 11 (2021) 2233–2257.
[34] A. Pandey et al., Cellulose nanocrystal stabilized emulsions for conformance control and fluid diversion in porous media, in: SPE Annual Technical Conference and Exhibition? SPE, 2018.
[35] L. Tliba, et al., Surface-modified silica nanoparticles for enhanced oil recovery in sandstone cores, J. Mol. Liq. (2024) 125815.
[36] X. Wang, et al., Fatty acid-asphaltene interactions at oil/water interface, Colloids Surf. A: Physicochem. Eng. Asp. 513 (2017) 168–177.

[37] K. Gurpreet, S. Singh, Review of nanoemulsion formulation and characterization techniques, Indian J. Pharm. Sci. 80 (5) (2018).
[38] Z. Abdulmohsein, B. Bai, P. Neogi, Emulsion stability of heavy oil with surfactants and nanoparticles, Improved Oil and Gas Recovery vol. 4 (2020).
[39] B. Rodier, et al., Controlling oil-in-oil pickering-type emulsions using 2D materials as surfactant, ACS Macro Lett. 6 (11) (2017) 1201–1206.
[40] F. Sagala, et al., Nanopyroxene-based nanofluids for enhanced oil recovery in sandstone cores at reservoir temperature, Energy Fuel 33 (2) (2019) 877–890.
[41] M. Shouxiang, N.R. Morrow, X. Zhang, Generalized scaling of spontaneous imbibition data for strongly water-wet systems, J. Pet. Sci. Eng. 18 (3–4) (1997) 165–178.
[42] S. Gogoi, S.B. Gogoi, Review on microfluidic studies for EOR application, J. Pet. Explor. Prod. Technol. 9 (2019) 2263–2277.
[43] S. Safarzadeh, A.L. Bila, O. Torsæter, Experimental Investigation of the Effect of Silica Nanoparticles on Interfacial Tension and Wettability during Low Salinity Water Flooding: A Micromodel Study, 2022.
[44] R. Khademolhosseini, et al., Synthesis of silica nanoparticles with different morphologies and their effects on enhanced oil recovery, Appl. Nanosci. 10 (2020) 1105–1114.
[45] A. Mandal, S. Kar, S. Kumar, The synergistic effect of a mixed surfactant (Tween 80 and SDBS) on wettability alteration of the oil wet quartz surface, J. Dispers. Sci. Technol. 37 (9) (2016) 1268–1276.
[46] A. Karimi, et al., Wettability alteration in carbonates using zirconium oxide nanofluids: EOR implications, Energy Fuel 26 (2) (2012) 1028–1036.
[47] Y. Moliner-Martínez, P. Campíns-Falcó, R. Herráez-Hernández, Influence of the presence of surfactants and humic acid in waters on the indophenol-type reaction method for ammonium determination, Talanta 69 (4) (2006) 1038–1045.
[48] B. Nair, Final report on the safety assessment of Sodium Alpha-Olefin Sulfonates, Int. J. Toxicol. 17 (5_suppl) (1998) 39–65.
[49] A. Badawi, et al., Novel quaternary ammonium hydroxide cationic surfactants as corrosion inhibitors for carbon steel and as biocides for sulfate reducing bacteria (SRB), Mater. Chem. Phys. 124 (1) (2010) 458–465.
[50] E.-J. Park, et al., Ammonium lauryl sulfate-induced apoptotic cell death may be due to mitochondrial dysfunction triggered by caveolin-1, Toxicol. In Vitro 57 (2019) 132–142.
[51] L.L. Schramm, L.L. Schramm, Surfactants: Fundamentals and Applications in the Petroleum Industry, Cambridge University Press, 2000.
[52] U. Zoller, P. Sosis, Handbook of Detergents, Part F: Production, CRC Press, 2008.
[53] S.C. Feifel, F. Lisdat, Silica nanoparticles for the layer-by-layer assembly of fully electro-active cytochrome c multilayers, J. Nanobiotechnol. 9 (2011) 1–12.
[54] Y. Cai, J. Xue, D. Polya, A Fourier transform infrared spectroscopic study of Mg-rich, Mg-poor and acid leached palygorskites, Spectrochim. Acta A: Mol. Biomol. Spectrosc. 66 (2) (2007) 282–288.
[55] L. Yadav, L. Yadav, Infrared (IR) spectroscopy, Org. Spectrosc. (2005) 52–106.
[56] Z. Hu, et al., Rheological properties of partially hydrolyzed polyacrylamide seeded by nanoparticles, Ind. Eng. Chem. Res. 56 (12) (2017) 3456–3463.
[57] S. Sandford, et al., The interstellar CH stretching band near 3.4 microns-constraints on the composition of organic material in the diffuse interstellar medium, Astrophys. J. 371 (1991) 607–620.
[58] J. Price, M. Crofton, Y.T. Lee, Vibrational spectroscopy of the ammoniated ammonium ions NH4+ (NH3) n (n= 1-10), J. Phys. Chem. 95 (6) (1991) 2182–2195.
[59] N. Sawitri, et al., Synthesis of proton-conducting membranes based on sulfonated polystyrene and bacterial cellulose. Journal of Physics: Conference Series, IOP Publishing, 2021.
[60] E. Knittle, W. Phillips, Q. Williams, An infrared and Raman spectroscopic study of gypsum at high pressures, Phys. Chem. Miner. 28 (2001) 630–640.
[61] D.S. Volkov, O.B. Rogova, M.A. Proskurnin, Organic matter and mineral composition of silicate soils: FTIR comparison study by photoacoustic, diffuse reflectance, and attenuated total reflection modalities, Agronomy 11 (9) (2021) 1879.
[62] A. Yaseen, et al., Synthesis and FTIR analysis of Cd doped nano Ni-aluminates, Asian J. Chem. Sci. 13 (5) (2023) 57–70.
[63] V. Sanchez Escribano, G. Busca, V. Lorenzelli, Fourier transform infrared spectroscopic studies of the reactivity of vanadia-titania catalysts toward olefins. 1. Propylene, J. Phys. Chem. 94 (26) (1990) 8939–8945.
[64] M. Khalfaoui, et al., New theoretical expressions for the five adsorption type isotherms classified by BET based on statistical physics treatment, J. Colloid Interface Sci. 263 (2) (2003) 350–356.
[65] M.L. Ojeda, et al., On comparing BJH and NLDFT pore-size distributions determined from N2 sorption on SBA-15 substrata, PCCP 5 (9) (2003) 1859–1866.
[66] A. Hethnawi, N.N. Nassar, G. Vitale, Preparation and characterization of polyethylenimine-functionalized pyroxene nanoparticles and its application in wastewater treatment, Colloids Surf. A: Physicochem. Eng. Asp. 525 (2017) 20–30.
[67] D.M. Clementz, Alteration of rock properties by adsorption of petroleum heavy ends: implications for enhanced oil recovery, in: SPE Improved Oil Recovery Conference? SPE, 1982.
[68] J.S. Buckley, C. Bousseau, Y. Liu, Wetting alteration by brine and crude oil: from contact angles to cores, SPE J. 1 (03) (1996) 341–350.
[69] T.L. Moore, et al., Nanoparticle colloidal stability in cell culture media and impact on cellular interactions, Chem. Soc. Rev. 44 (17) (2015) 6287–6305.
[70] N. Kobayashi, H. Izumi, Y. Morimoto, Review of toxicity studies of carbon nanotubes, J. Occup. Health 59 (5) (2017) 394–407.
[71] W. Anderson, Wettability literature survey-part 2: Wettability measurement, J. Petrol. Tech. 38 (11) (1986) 1246–1262.
[72] F. Wang, Z. Qu, Z. Xue, A study on emulsion flow in porous media with micromodel, J. Northwest. Univ. (Nat. Sci. Ed.) 33 (2003) 603–607.
[73] F. Yakasai, et al., Current developments and future outlook in nanofluid flooding: a comprehensive review of various parameters influencing oil recovery mechanisms, J. Ind. Eng. Chem. 93 (2021) 138–162.
[74] J. Mariyate, A. Bera, Recent progresses of microemulsions-based nanofluids as a potential tool for enhanced oil recovery, Fuel 306 (2021) 121640.
[75] X. Hou, J.J. Sheng, Fabrication of a spontaneous emulsification system for low-permeable oil reservoirs and study of an enhanced oil recovery mechanism based on the nuclear magnetic resonance method, Energy Fuel 36 (1) (2021) 227–238.